HP-tectono-metamorphic evolution of the Internal Piedmont Zone in Susa Valley (Western Alps): New petrologic insight from garnet+chloritoid –bearing micaschists and Fe-Ti metagabbro

DR. STEFANO GHIGNONE (Orcid ID : 0000-0002-1295-6291)

DR. CHIARA GROPPO (Orcid ID : 0000-0002-4174-6613)

Article type : Original Article

HP-tectono-metamorphic evolution of the Internal Piedmont Zone in Susa Valley (Western Alps): New petrologic insight from garnet+chloritoid –bearing micaschists and Fe-Ti metagabbro

Ghignone S.[1]*, Borghi A.[1], Balestro G.[1], Castelli D.[1], Gattiglio M.[1], Groppo C.[1]

[1] Dipartimento di Scienze della Terra, Università degli Studi di Torino, Via Valperga Caluso 35, I-10125 Torino, Italy

* Corresponding author: s.ghignone@unito.it

Abstract

New petrologic data from meta-ophiolites exposed in a relatively poorly known sector of the Western Alps (i.e. Susa Valley, Internal Piedmont Zone) are reported. Garnet + chloritoid -bearing phengitic micaschist and Fe-Ti metagabbro preserving eclogite-facies assemblages have been investigated in detail to constrain the HP-tectono-metamorphic evolution of meta-ophiolites in the study area. Microstructural investigations allowed to identify different assemblages related to different tectono-metamorphic stages, whose pressure-temperature (P-T) conditions of the HP stages were constrained using the pseudosection modelling approach combined with multi-equilibrium thermobarometry. Four main metamorphic stages have been recognized: i) an Alpine peak-P stage (M1a), which reached the HP-UHP eclogite-facies boundary (P=25-29 kbar, T=460-510°C); ii) a slightly prograde decompression stage (M1b), still under eclogite-facies conditions (P=21-25 kbar, T=500-530°C); iii) a greenschist-facies re-equilibration stage (M2) ; iv) a nearly isobaric late heating stage (M3), developed at the boundary between greenschist- and amphibolite-facies conditions. The new P–T path inferred for the HP phases recorded by the studied meta-ophiolites is compatible with that reported from other meta-ophiolite units in the Western Alps, i.e. the Zermatt-Saas ophiolite to the north and the Monviso ophiolite to the south, confirming that subduction of the Tethys

oceanic lithosphere occurred at similar P-T regimes all along its length. The comparison with the tectonic evolution of the adjacent Dora Maira continental crustal unit suggest that the early exhumation of eclogitized oceanic crust likely occurred along the plate interface in the subduction channel, without the buoyancy contribution of continental crust.

Keywords: Alpine metamorphic evolution, meta-ophiolite, phase equilibria modelling, Piedmont Zone, Western Alps

1. Introduction

Ophiolites represent remnants of oceanic lithosphere involved in processes of subduction - obduction and subsequently stacked in orogenic belts, and their study is useful for reconstructing the geodynamics of collisional chains. In the case of the Western Alps, meta-ophiolites preserve traces of long and complex tectonic histories, from the opening of the Piedmont-Ligurian Ocean in the Jurassic time, to the Late Cretaceous-Paleocene subduction and subsequent Eocene-Oligocene exhumation (see e.g., Butler, Beaumont, & Jamieson, 2013, and Dal Piaz, Bistacchi, & Massironi, 2003). Based on lithostratigraphy and/or Alpine metamorphic evolution, several meta-ophiolite units have been distinguished in the Piedmont Zone of the Western Alps (Balestro, Festa, & Dilek, 2019; Barfety, Lemoine, De Graciansky, Tricart, & Mercier, 1995; Deville, Fudral, Lagabrielle, Marthaler, & Sartori, 1992; Elter, 1971; Festa, Balestro, Dilek & Tartarotti, 2015; Fudral et al., 1994; Lagabrielle et al., 1984; Martin, Tartarotti, & Dal Piaz, 1994 and references therein). A still debated issue concerns whether the pressure–temperature (P-T) conditions registered by Alpine meta-ophiolites are largely uniform or if different units of the Piedmont Zone actually recorded different P–T peak conditions and underwent different subduction and exhumation paths (Beltrando, Compagnoni, & Lombardo, 2010, with references).

This paper aims at improving our knowledge about the tectono-metamorphic evolution of ophiolitic rocks exposed in a sector of the Western Alps (i.e. the Susa Valley, NW Italy; **Figures 1-2**), which is significantly less known with respect to other meta-ophiolites exposed more to the north (i.e. the Zermatt-Saas meta-ophiolite; e.g. Angiboust, Agard, Jolivet, & Beyssac, 2009; Bucher, Fazis, De Capitani, & Grapes, 2005) and to the south (i.e. the Monviso meta-ophiolite Complex; e.g. Angiboust, Langdon, Agard, Waters, & Chopin., 2012; Balestro et al., 2014; Groppo & Castelli, 2010; Locatelli, Verlaguet, Agard, Federico & Angiboust, 2018; Lombardo et al., 1978).

In fact, the prograde and peak P-T conditions experienced by meta-ophiolitic rocks in the study area are especially poorly constrained, as previous studies date back to over 20-30 years ago, and mostly rely on conventional thermobarometric methods (e.g. Agard , Jolivet, & Goffè, 2001; Pognante & Kienast, 1987). Different lithologies exposed at different distances from the major shear zone have been investigated. The obtained results provide new insights on the tectono-metamorphic evolution of a relatively poorly known

sector of the meta-ophiolites of the Western Alps, confirming that subduction of the Tethys oceanic lithosphere occurred at similar P-T regimes all along its length. It has been also observed that the onset of the exhumation of the oceanic unit started from greater depths than the adjacent Dora Maira continental crustal unit and before the tectonic coupling of the two units. This implies that the oceanic units were exhumed, at least at the beginning, through mechanisms independent from buoyancy-driven exhumation processes.

2. Geological setting

The Western Alps (**Figure 1**) are a collisional belt, resulting from convergence between the upper Adriatic and lower European plates, and the interposed Ligurian–Piedmont oceanic basin (i.e., the Alpine Tethys: see e.g., Agard, Yamato, Jolivet, & Burov, 2009; Ernst & Dal Piaz, 1978; Lemoine & Tricart 1986; Vissers, Van Hinsbergen, Meijer, & Piccardo, 2013). The axial sector of the belt, consisting of the most deformed (U)HP tectono-metamorphic units, corresponds to an exhumed fossil subduction-complex, which was overthrusted on the European foreland (see e.g. Ricou & Siddans, 1986; Schmid, Kissling, Diehl, van Hinsbergen, & Molli, 2017).

Based on different metamorphic evolution and lithostratigraphic setting, meta-ophiolite units of the Western Alps have been classically distinguished into Zermatt-like units (i.e., Internal Piedmont Zone, IPZ) and Combin-like units (i.e., External Piedmont Zone, EPZ) (Bearth 1967).

The IPZ is mainly composed of meta-ophiolite rocks with a thin metasedimentary cover (see e.g., Balestro et al., 2018; Locatelli, Federico, Agard, & Verlaguet, 2019; Tartarotti, Festa, Benciolini, & Balestro, 2017 and references therein), and it was metamorphosed under eclogite-facies conditions, followed by a strong greenschist-facies overprint (see e.g., Bucher et al., 2005; Reddy Wheeler, & Cliff, 1999 and references therein). Peak P-T conditions in the range of 520–560 °C and 22–25 kbar (Angiboust et al., 2009) and of slightly different 550-600°C and 25-30 kbar (Bucher et al., 2005) have been proposed for the Zermatt-Saas meta-ophiolites. Similar peak P-T conditions (i.e. of roughly 25 kbar and 550°C) have been constrained for the southernmost Monviso meta-ophiolite Complex (Angiboust et al., 2012; Balestro et al., 2014; Groppo & Castelli, 2010; Locatelli et al., 2018). The occurrence of coesite and microdiamonds in a small unit within the Zermatt-Saas meta-ophiolites (i.e., the Cignana Unit; Frezzotti, Selverstone, Sharp, & Compagnoni, 2011; Luoni, Rebay, Spalla & Zanoni, 2018; Reinecke 1991, 1998) point to UHP peak conditions (P>32 kbar; T=590-605°C, Groppo, Beltrando, & Compagnoni, 2009).

The EPZ mainly consists of a thick meta-sedimentary cover (i.e., calcschist) with ophiolitic bodies (i.e., metabasalt, serpentinite and minor metagabbro) as reported by e.g., Caby (1981). These rocks show a pervasive greenschist-facies metamorphic overprint, with blueschist-facies relics (Agard et al., 2001; Schwartz, Tricart, Lardeaux, Guillot, & Vidal, 2009 and references therein). P-T conditions in the range of 12–13 kbar and 425–475 °C (Combin Unit; Cartwright & Barnicoat 2002; Negro, Bousquet, Vils, Pellet,

Hänggi-Schaub, 2013), ~500 °C, 15 kbar (Combin Unit; Angiboust, Glodny, Oncken, & Chopin, 2014; Negro et al., 2013), 16-19 kbar and 400-480°C (Maurienne area; Plunder, Agard, Dubacq, Chopin, & Bellanger, 2012), 12–20 kbar and 300–450 °C (northern Queyras Complex; Agard et al. 2001, and Michard, Avigad, Goffé, & Chopin, 2003) and 8–14 kbar, 300–475 °C (southern Queyras Complex; Tricart & Schwartz 2006) have been constrained in different units of the EPZ. The metamorphic re-equilibration developed under greenschist-facies conditions (5–9 kbar and 250–450 °C in the Combin Unit, Reddy et al., 1999; 5–8 kbar and 250–450 °C in the Queyras Complex, Agard, Monie, Jolivet, & Goffe, 2002).

The age of the eclogitic peak recognized in the IPZ encompasses values between 60 and 45 Ma, while the age of the greenschist-facies re-equilibration ranges between 43 and 32 Ma (Agard et al., 2002; Amato, Johnson, Baumgartner, & Beard, 1999; Bowtell, Cliff, & Barnicoat, 1994; Cliff, Barnicoat, & Inger, 1998; Duchêne et al. 1997; Federico, Capponi, Crispini, Scambelluri, & Villa, 2005; Monié and Philippot, 1989; Rubatto and Hermann, 2003; Rubatto, Gebauer, & Fanning, 1998). The age of peak-P conditions in EPZ ranges between 57 and 38 Ma, and the subsequent greenschist-facies re-equilibration encompasses values between 39 and 35 Ma (Dal Piaz et al, 2001; Reddy et al., 1999; Rosenbaum & Lister, 2005; Weber et al., 2015). The age of tectonic juxtaposition between IPZ and EPZ has been recently dated at 38-35 Ma by Angiboust & Glodny (2020), in the Monviso and Rocciavrè area. These geochronological data are coherent with those obtained by other authors along the Western Alpine belt in the same structural position (see e.g., Reddy et al., 1999).The study area (**Figure 2a**) is located in the Susa Valley, wherein different tectonic units are exposed. These tectonic units, from lower to higher structural levels, correspond to (i) the northern sector of the Dora Maira (DM) European continental margin unit, (ii) the IPZ and (iii) the EPZ. In the Susa Valley, the DM and the overlying IPZ were folded together during early exhumation-related deformation phase and are both separated by the EPZ through the Susa Shear Zone (SSZ; Gasco, Gattiglio, & Borghi, 2013; Ghignone & Gattiglio, 2013: Ghignone et al., 2020; **Figure 2b**).

The northern sector of the DM consists of a polymetamorphic basement intruded by Permian granitoids and covered by Permo-Mesozoic metasediments (see e.g., Cadoppi et al., 2002; Sandrone, Cadoppi, Sacchi, & Vialon, 1993). The DM reached eclogite-facies peak-P conditions (T=515–525°C, P=18–20 kbar, Gasco, Gattiglio, & Borghi, 2011) and was subsequently re-equilibrated under greenschist- to amphibolite-facies conditions.

The IPZ tectonically overlies the DM (i.e., the Orsiera-Rocciavrè Complex of Pognante, 1979; and the Bassa Val di Susa-Valli di Lanzo-Monte Orsiera Unit of Cadoppi et al., 2002), and consists of serpentinite, metagabbro, metabasite and metasediments (Balestro, Cadoppi, Perrone, & Tallone, 2009; Leardi & Rossetti, 1985; Nicolas, 1967; Pognante, 1979; Pognante, 1980).

Serpentinite is both massive and strongly foliated (i.e., serpentine schist), metabasite locally retain relics of breccia- and pillow-lava structures, and metasediments consist of Mn-rich quartzite, impure marble,

micaschist and calcschist. The IPZ experienced eclogite-facies peak metamorphic conditions, as proved by occurrences of Fe-Ti metagabbro with well-preserved garnet-omphacite-glaucophane-rutile assemblages (Lombardo & Pognante, 1982; Pognante, 1984; Pognante & Kienast, 1987). Quantitative estimates of peak P-T conditions were given by Agard et al. (2001; 2002) at P=18-20 kbar, T=450°-520°C using conventional thermobarometry, whereas P-T data obtained using modern petrological approaches (i.e., pseudosections) are lacking so far.

EPZ consists of a thick meta-sedimentary succession mostly consisting of calcschist with bodies of metabasalt, serpentinite, paragneiss, quarzite and micaschist (i.e., the Schistes Lustrés of Deville et al., 1992, and the Puy-Venaus Unit of Cadoppi et al., 2002). Blueschist-facies peak metamorphic conditions were constrained by occurrences of glaucophane-phengite-rutile mineral assemblage in metabasite, and carpholite-bearing and chloritoid-bearing assemblages in calcschist. The P–T conditions vary rather continuously across the Schistes Lustrés complex in the Cottian Alps, from 350° C and 12–13 kbar to 500° C and 18–20 kbar (Agard et al., 2001), as exemplified by the progressive eastward increase of the phengitic substitution in carpholite- or chloritoid-bearing assemblages.

3. Methods

3.1. Fieldwork

A detailed geological study at the meso-scale was carried out in the Susa Valley (Italian Western Alps), wherein the geometric relationships between different tectono-metamorphic units of the axial sector of the orogen are well-exposed. Fieldwork and structural analysis allowed the selection of the most appropriate samples for this study.

Structural observations, collected at the mesoscale, were used to define the tectonic setting of the IPZ. Further details on mesoscale structural and stratigraphic observations are provided by Ghignone et al. (2020).

3.2. Petrography and mineral chemistry

Studied samples belong both to the meta-ophiolitic basement and to the metasedimentary cover of the IPZ. Detailed petrologic study was performed on two metapelites and one Fe-Ti metagabbro (see *Section 5*) and the results are summarized in **Table 2**. The rock-forming minerals were analysed with a JEOL IT300LV Scanning Electron Microscope at the Department of Earth Sciences, University of Torino. The instrument was equipped with an energy dispersive spectrometry (EDS) Energy 200 system and an SDD X-Act3 detector (Oxford Inca Energy). Operating conditions were: 15kV accelerating voltage, 5nA probe current, 1 μs EDS process time, 10^5 cnts/s, 30 s counting time. SEM-EDS quantitative data were acquired and processed using the Microanalysis Suite Issue 12, INCA Suite version 4.01; natural mineral standards were used to calibrate the raw data; the ΦρZ correction (Pouchou & Pichoir, 1988) was applied. Representative

SEM-EDS analyses of garnet, clinopyroxene, amphibole, white mica (Wm), biotite, chlorite, plagioclase and epidote are reported in **Table S1**. Fe^{+3} in garnet has been estimated by stoichiometry.

High-resolution multispectral maps (**Figure 4**) of the entire thin sections (almost 4 x 2 cm) used for deriving the effective bulk compositions of the investigated samples were obtained using the same SEM instrument. Operative conditions used for mapping entire thin section were: 15kV accelerating voltage, 5nA probe current, 1 μs EDS process time, 10^5 cnts/s, 2.5 μm point step, 1 msec dwell time. The row data were processed using the MultiSpec© software in order to obtain the modal compositions.

Mineral abbreviations in the text, figures and tables are from Whitney & Evans (2010).

3.3. Thermodynamic modelling

The P-T isochemical phase diagram (pseudosection modelling) approach was applied to two metapelites (VS17 and MOM15) and on one Fe-Ti metagabbro (VS20). Bulk rock compositions of these samples (**Table 1**) were calculated by combining the mineral proportions obtained from the quantitative modal estimate of SEM-EDS multispectral maps with mineral chemistry acquired at SEM-EDS.

The study focuses on metapelites (i.e., garnet-chloritoid -bearing phengitic micaschist) because they are widely diffused in the investigated units and well preserve the HP assemblages, instead of metagabbro, which preserves abundant magmatic relics and is characterized by coronitic structures, index of lack of equilibrium.

The fractionation effects on the bulk composition due to the growth of strongly zoned garnet porphyroblasts were considered for sample VS17, which is characterized by garnet porphyroblasts with a pronounced prograde zoning (see *Section 6*). For this sample, two pseudosections were therefore calculated in order to model: (i) the P-T conditions for the growth of garnet core (measured bulk composition: MBC), (ii) the P-T conditions for the growth of garnet rim (MBC minus garnet cores). Chemical fractionation effects were not considered for samples MOM15 and VS20 because garnet rims were either re-equilibrated by diffusion (sample MOM15) or partially replaced by other phases (sample VS20) during the post-peak metamorphic evolution.

The pseudosections were calculated in the systems MnNCKFMASH (MnO-Na_2O-CaO-K_2O-FeO-MgO-Al_2O_3-SiO_2-H_2O; samples VS17 and MOM15) and MnNCFMASH (sample VS20) using Perple_X 6.8.4 (Connolly, 1990, 2005, 2009), the internally consistent thermodynamic database of Holland & Powell (2011) (ds62) and the equation of state for H_2O of Holland & Powell (1998). Fluid saturated conditions were assumed, and the fluid was considered as pure H_2O (aH_2O=1). This last assumption is realistic for the studied samples, because of the large occurrence of hydrous phases, the absence of primary carbonates and sulphides. SiO_2 was considered in excess for the metapelitic samples (VS17 and MOM15), because of the widespread occurrence of quartz both in the matrix and included in garnet, but not for the metabasic sample (VS20). Fe^{3+} was neglected in the pseudosections calculated for metapelitic samples, because Fe^{3+}-rich

oxides are absent and the amount of Fe^{3+} in the analyzed minerals is very low. The occurrence of graphite in the metapelites further confirms low oxidation conditions. The influence of Fe^{3+} on the pseudosection topology and on the constrained P-T evolution was explored for the metabasic sample VS20 through the calculation of isobaric T-X(Fe_2O_3) and isothermal P-X(Fe_2O_3) pseudosections. TiO_2 was not included in the calculation because rutile is the only Ti-bearing phase stable at HP conditions in all the samples. K_2O was neglected in the pseudosection calculated for sample VS20 because K-bearing phases are lacking.

The following solid solution models were used: biotite, chlorite, chloritoid, garnet, staurolite, white mica (White, Powell, Holland, Johnson, & Green 2014), clinopyroxene (Green, Holland, & Powell, 2007), amphibole (Green et al., 2016), feldspar (Fuhrman & Lindsley, 1988), carpholite (Smye, Greenwood, & Holland, 2011) and talc (ideal model). Quartz, lawsonite, kyanite and zoisite were considered as pure phases.

4. Tectonostratigraphic setting of the study area

The IPZ in the Susa Valley consists of a meta-ophiolitic basement with an overlying meta-sedimentary cover (see Ghignone et al. 2020). The meta-ophiolitic basement is composed of massive serpentinite, serpentine schist, metabasite and metagabbro (**Figure 3a-b**).

The latter occur in hundreds meter-thick bodies, either as sub-rounded and boudinated bodies (few meters in size) within serpentinites (**Figure 3a**), or as tectonic slices wrapped by mylonitic foliation along the main tectonic contacts. Fe-Ti metagabbro are massive, coarse- to medium-grained and locally banded, with a weak foliation defined by preferential mineral orientation. The eclogitic mineral assemblage, where preserved, consists of clinopyroxene (omphacite), garnet, Na-amphibole (glaucophane) and millimetric-thick stripes of rutile.

Metabasites overlies the serpentinites and the embedded metagabbro, and are hundreds of meters thick.

Along the shear zones, however, metabasites occur as discontinuous bodies (few meters to decameters in thickness) wrapped by mylonitic calcschists. This lithology is usually massive, greenish in colour, fine-grained, and it locally exhibits banded structure (**Figure 3c**). A weak and spaced foliation is defined by the iso-orientation of elongated minerals (epidote, amphibole, and locally white mica).

The metasedimentary cover mostly consists of pervasively foliated calcschists. The lowermost portion of the metasedimentary succession is characterized by the occurrence of up to few-meters thick layers of quartzite, micaschist (i.e. metapelitic rocks) and grey marbles (**Figure 3c**). Micaschist are garnet- and chloritoid-bearing and consist of alternating mm-thick fine-grained phyllosilicates levels (white mica, chlorite and graphite) and quartz-rich levels.

The meta-ophiolites and related metasedimentary cover were deformed during four regional phases (from D1 to D4), and two shearing events (T1 and T2) developed along the Susa Shear Zone (SSZ), along which

IPZ and EPZ juxtaposed. An early event, referred to a pre-D1 deformation stage by Gasco et al. (2013), rarely occurs as relict structural elements in Fe-Ti metagabbro and quarzite.

Structures related to the D1 phase are discontinuously preserved and correspond to the S1 axial plane foliation and to rootless isoclinal folds with elongated limbs, sharp hinges and asymmetric geometry (**Figure 3d**).

The main structures developed in the study area are related to the D2 deformation phase. D2 folds exhibit isoclinal profile and developed a pervasive axial plane foliation (S2), which represents the main (regional) foliation (**Figure 3d**). D2 is an almost transpositive deformation event and leads to parallelization of oldest surfaces to the S2. Domains escaped from D2 transposition, preserve previous D1 microstructures and related mineral assemblages (i.e., HP eclogitic phases).

The first shearing event (T1) gave rise to a thick shear zone (SSZ), marked by a mylonitic foliation (SM, **Figure 3e**), and overprinted and transposed both the S2 and the previous lithological banding. Evidences of the subsequent D3 phase mainly consist of D3 folds, which are asymmetric and, locally, with overturned short limbs. The second shearing event (T2) developed discrete shear bands (**Figure 3f**), that crosscut the previous SM mylonitic foliation. D4 is the later regional phase, characterized by variably open to gentle folds. D4 deformation phase is nearly coeval with the T2, as reported in Ghignone et al., 2020.

On the basis of microstructural relationships four Alpine metamorphic stages have been distinguished (**Table 2**): i) the peak-pressure metamorphic event (M1a) only preserved as mineralogic relics inside garnet and omphacite porphyroblasts; ii) a first decompressional event (M1b) still developed under the eclogite-facies and related to D1 deformation phase, discontinuously preserved at the mesoscale iii) the tectono-metamorphic event M2 responsible for the development of the main regional foliation (D2 phase), under greenschist facies conditions iv) finally, re-equilibration occurred under upper greenschist to amphibolite facies conditions (M3).

5. Petrography and mineral chemistry

More than 30 thin sections of different lithologies (mainly Fe-Ti-metagabbro, metabasite and micaschist) belonging to the IPZ were observed under optical microscope, among which 20 have been collected within the SSZ; their petrographic features are briefly summarized here, with major emphasis on those lithologies that have been used for constraining peak metamorphic conditions (i.e. Fe-Ti metagabbro and micaschist). Mineral chemical data are discussed for the three samples (Fe-Ti metagabbro: VS20; micaschist: VS17 and MOM15) that have been selected for further petrological investigations. Sample locations are reported in **Figure 2,** and GPS coordinates in **Table 1**.

5.1 Fe-Ti metagabbro

In the SSZ, Fe-Ti metagabbro are coarse-grained, poorly deformed, massive rocks, preserving abundant relics of the magmatic assemblage (mostly augitic clinopyroxene and ilmenite). The eclogitic assemblage mostly develops in coronitic microstructures (see e.g. Pognante, 1985): omphacite forms a continuous rim around augite relics, garnet is concentrated in mm-thick coronas around clinopyroxene domains and rutile rims ilmenite relics. The former plagioclase domains of the igneous protolith are pervasively replaced by retrograde phases (clinozoisite/epidote, white micas). The eclogitic assemblage additionally includes minor amounts of glaucophane, occurring both in the matrix and as fine-grained inclusions in garnet, and lawsonite, pseudomorphically replaced by fine-grained, lozenge-shaped aggregates of epidote + paragonite preserved as inclusions in garnet and/or within the former plagioclase domains in the matrix. Evidences of the retrograde re-equilibration are: (i) symplectites (mostly fine-grained albite + tremolite, locally rimmed by very fine-grained albite + diopside) partially replacing omphacite at the rim, (ii) NaCa- and Ca-amphiboles growing at the rim of glaucophane, (iii) epidote + paragonite pseudomorphs after lawsonite, and (iv) chlorite, partially replacing garnet along fractures and at the rim. The preservation of igneous relics is a clear evidence that equilibrium conditions were not attained in these Fe-Ti metagabbro during eclogitic metamorphism; for this reason, these coronitic Fe-Ti-metagabbro were not selected for further petrological investigations.

In contrast to what observed within the SSZ, far from the SSZ Fe-Ti metagabbro form larger (i.e. up to a hundred meters) bodies, hosted within serpentinite. These are weakly foliated and locally banded rocks, with alternating leucocratic and melanocratic domains related to metamorphic layering. The eclogitic assemblage is generally well preserved, with few evidences of re-equilibration at lower pressures. Magmatic relics are mostly absent or limited to few ilmenite relics. The texture is generally gneissic, with garnet, omphacite ± glaucophane porphyroblasts wrapped by a fine-grained, weakly foliated matrix, mostly consisting of epidote, chlorite and green amphibole.

5.1.1 Sample VS20

Sample VS20 is representative of the Fe-Ti metagabbro exposed far from the SSZ (see **Figure 2** for sample location) and shows a well-equilibrated eclogitic assemblage. It is a medium- to coarse-grained, slightly foliated Fe-Ti metagabbro. Its eclogitic assemblage consists of garnet, omphacite, glaucophane and rutile (see **Figure 4a**). The coarse-grained eclogitic minerals are set in a fine-grained matrix consisting of green amphibole, chlorite, epidote and albite, derived from re-equilibration at lower pressures.

Garnet occurs as mm to hundreds of μm sized, partly fractured, crystals. It includes abundant omphacite, rutile, glaucophane (**Figure 5a**) and minor lozenge-shaped pseudomorphs after former lawsonite, now consisting of fine-grained epidote + paragonite (**Figure 5b**). Microstructurally, garnet is pre-kinematic with respect to the main foliation. Garnet is rich in almandine and grossular components, and it is weakly zoned, with spessartine and grossular decreasing and almandine and pyrope increasing from core to rim (core:

Alm_{70-74}, Sps_{4-6}, Prp_{3-6}, Grs_{11-19}, Adr_{0-2}; rim: Alm_{77-79}, Sps_{0-2}, Prp_{6-9}, Grs_{4-7}, Adr_{0-4}) as reported in **Figure 7a-b-c-d**.

Omphacite occurs as mm- to sub-mm sized crystals, partially re-equilibrated along cleavages and at the rim (**Figure 5c-d**). Three generations of omphacite have been distinguished based on their microstructural relations and compositions (**Figure 7g**): (i) a bright-green OmpI (Jd_{20-30}), (ii) a pale-green OmpII (Jd_{31-38}), and (iii) a dark-green OmpIII (Jd_{39-49}). OmpI and OmpII both occur in the core of omphacite crystals and define a patchy zoning (**Figure 5d**); their relationship is ambiguous (i.e. it is not clear whether one omphacite replaces the other, or if OmpI and OmpII are in equilibrium), but their systematic occurrence in the core of omphacite crystals suggests that they both have a prograde nature. OmpIII systematically occurs as a discontinuous rim around the patchy zoned OmpI + OmpII core. Moreover, OmpIII systematically occurs as inclusion in garnet. Omphacite includes very-fine grained (10-20 μm in size) flakes of talc (**Figure 5e**), glaucophane and rutile. Omphacite is partially replaced at the rim by a fine-grained symplectite, consisting of actinolite + albite (**Figure 5f**).

A bluish to pale-purple sodic-amphibole (glaucophane) also occurs in the eclogitic assemblage, either as medium- to coarse-grained crystals in the matrix or as inclusions in garnet and omphacite. Three later generations of amphibole have been further recognised (**Figure 5g**), reflecting different stages of the retrograde evolution; they grew around previous amphibole generations, within the fine-grained matrix, and/or in the symplectites around omphacite. These retrograde amphiboles are (**Figure 7h**): (i) a bright-green sodic-calcic amphibole (katophorite), (ii) a pale-green calcium-amphibole (actinolite), (iii) a brownish calcic-amphibole (hornblende-pargasite).

Paragonite rarely occurs in this sample and it is limited to the pseudomorphs after former lawsonite preserved as inclusions within garnet. In these pseudomorphs, paragonite is systematically associated to epidote (**Figure 5b**). Epidote also occurs in the fine-grained matrix and it is generally zoned, with a clinozoisite core (Ep_{9-29}) and an epidote rim (Ep_{64-96}).

Plagioclase occurs either as poikiloblasts in the matrix or as fine-grained crystals associated to actinolite in the symplectites replacing omphacite. Plagioclase poikiloblasts are weakly zoned, with a large core of almost pure albite (An_{0-9}) and a thin rim slightly enriched in Ca (oligoclase, An_{11-15}; see **Table S1**). Chlorite occurs in the fine-grained matrix, where it defines the weak gneissic foliation, and partially replaces garnet along fractures and at the rim. Its composition is quite homogeneous, ranging from pycnoclorite to ripidolite.

The mineral assemblages – deformation diagram (blastesis-deformation) reconstructed for this sample (**Table 2**) highlights the relations between the four main metamorphic events (M1a to M3), each one characterized by its own equilibrium assemblage, and the main structural events (pre-D1 to D3, respectively, see *Section 4*).

5.2 Metapelite

Metapelitic rocks represent the lowermost term of the IPZ meta-sedimentary cover, often defining the basement/cover boundary (as reported in **Figure 3c**). Fine- to medium-grained micaschist crop out in meters -thick layers, showing a well-developed foliation (i.e. either S2 foliation or SM mylonitic foliation) defined by the preferred orientation of white mica ± chlorite. Preserved relics of the eclogitic assemblage include variable amounts of garnet, phengite, chloritoid and rutile; glaucophane and lawsonite have been inferred as part of the HP assemblage, although they have been completely replaced by retrograde phases (see below).

Two different samples of micaschist have been selected for further petrological investigations and are described in detail in the following. Both samples are exposed within the SSZ (see **Figure 2** for sample locations), but they are characterized by different degrees of deformation. In sample VS17, the main foliation is the S2, locally deformed by T2-related C-planes (S-C structure); sample MOM15 has been collected along the T1-related shear zone, and the main foliation coincides with the SM mylonitic foliation.

5.2.1 Sample VS17

This micaschist shows a well-developed S2 foliation defined by mm-spaced micaceous domains alternated to quartz-rich domains. The eclogitic assemblage consists of garnet, phengite, minor chloritoid and accessory rutile (see **Figure 4b**). Glaucophane and lawsonite are not preserved, but their former occurrence in the eclogitic assemblage has been inferred from the presence of their pseudomorphs. Retrograde mineral phases are mostly represented by muscovite and chlorite, with minor biotite, plagioclase and epidote.

Garnet porphyroblasts (1-3 mm in size) are pre-kinematic with respect to the main foliation, being enveloped by the S2 schistosity (**Figure 6a**). They are crowded with inclusions (mostly of quartz, chloritoid and graphite, with few phengite and lozenge-shape pseudomorphs after former lawsonite, now consisting of epidote + paragonite, **Figure 6c**), locally oriented to define an internal foliation (i.e., S1 foliation and rootless transposed folds).

Garnet is partially replaced by chlorite and biotite along fractures and rims. Garnet porphyroblasts show a marked, bell-shaped zoning, characterized by: (i) an inner core, with very high amount of spessartine (Alm_{28-40}, Sps_{51-60}, Prp_{1-2}, Grs_{1-3}, Adr_{2-3}); (ii) an outer core, characterized by a rapid decrease of spessartine outward, counterbalanced by an enrichment in almandine, pyrope and grossular (outer core: Alm_{41-77}, Sps_{10-30}, Prp_{2-6}, Grs_{2-5}, Adr_{1-3}); (iii) a rim marked by a further significant decrease of spessartine outward counterbalanced by the almandine, pyrope and grossular increase (rim: Alm_{78-86}, Sps_{1-3}, Prp_{4-7}, Grs_{4-7}, Adr_{1-2}, see **Figure 7a-b-c-e**). The garnet inner cores are volumetrically minor and highly scattered throughout the sample (i.e. they have not been observed in all garnet porphyroblasts), thus suggesting that their growth was controlled by local (at sub-millimetric scale) enrichment in Mn of the bulk rock composition, rather

than to the prograde P-T conditions. Garnet zoning trend is reported in **Figure 7e**, in the rim-to-rim chemical profile.

Potassic white mica is the most abundant mineral in this sample. Based on the microstructural position and chemical composition, two different white mica generations (**Figure 7i**) have been recognised: (i) a phengite with high- to medium-Si contents spread on a wide compositional range (Si=3.38-3.62 a.p.f.u.) mostly defines the S1 foliation, preserved as iso-oriented cores of coarser-grained mica flakes partially wrapped by the S2 foliation (**Figure 6d**); (ii) a low-Si (Si=3.10-3.29 a.p.f.u.) muscovite defines the main S2 foliation. Phengite was likely already stable earlier than the development of the S1 foliation (i.e. during the prograde and M1a events; **Table 2**), thus explaining its wide compositional range; however, a reliable discrimination between these different phengite generations was not possible on a microstructural basis.

Chloritoid only occurs as fine-grained (100-200 μm in size) inclusions within garnet (both in the garnet outer core and in garnet rim; **Figure 6e**), usually associated with phengite, whereas it is absent in the matrix. Its composition is quite homogeneous, with X_{Mg} values between 0.09 and 0.14 (**Table S1**). Lozenge-shaped, fine-grained aggregates of albite, chlorite and greenish biotite in the matrix (**Figure 6b**) are interpreted as pseudomorphs after a former Na-rich phase (likely glaucophane and/or jadeite). Several Authors interpreted similar such pseudomorphs, widely occurring in rocks of the DM massif, as the result of the destabilization of glaucophane during re-equilibration stages in a non-isochemical system (Borghi, Cadoppi, Porro, & Sacchi, 1985; Chopin, Henry & Michard, 1991; Groppo et al., 2019; Sandrone & Borghi, 1992).

Chlorite occurs in the foliation domains and it defines the S2 foliation together with muscovite; it also replaces garnet along fractures and at the rim (**Figure 6c**). Its composition is quite homogeneous, ranging from pycnoclorite to ripidolite.

Two types of biotite have been distinguished according to their pleochroism: (i) a brownish to yellow biotite replaces garnet and chlorite, and (ii) a dark-green to pale-green biotite occurs in lozenge-shaped pseudomorphs after former glaucophane and/or jadeite (**Figure 6b**). Despite their different colours, the two biotite types have similar, quite variable, compositions (Al = 2.7-3.7 a.p.f.u., X_{Fe} = 0.5-0.8; Ti = 0.05-0.19 a.p.f.u.). Plagioclase is rare and mostly occurs close to garnet porphyroblasts, where it seems to replace former paragonite-rich domains. It is almost pure albite (An_{0-4}). Epidote mostly occurs in the pseudomorphs after lawsonite included in garnet (**Figure 6c**). It locally occurs also in the matrix, scattered within white mica layers. Its composition is quite homogeneous (Ep_{62-80}). Rutile, titanite, apatite and tourmaline are accessory minerals. Rutile in the matrix is partially replaced by titanite. The mineral assemblages – deformation diagram (blastesis-deformation) reconstructed for this sample (**Table 2**) allow recognising four main metamorphic events (M1a to M3), each one characterized by its own equilibrium assemblage, and to associate them with the main structural events (D1 to D3, see *Section 4*). Evidence of pre-D1 deformation

stage were not observed in this sample although metamorphic relics of prograde and P-peak (M1a) conditions are present.

5.2.2 Sample MOM15

Sample MOM15 is a mylonitic micaschist, consisting of cm-thick micaceous levels alternated with thinner quartz-rich domains (see **Figure 4c**). The eclogitic assemblage is defined by the same phases as in sample VS17 (i.e. garnet, phengite, chloritoid and rutile + pseudomorphosed lawsonite), but in different modal amounts. Chlorite and muscovite are retrograde phases, and graphite and tourmaline are accessory minerals. The main mylonitic foliation SM transposes earlier foliations and pervasively re-orient white micas defining both S1 and S2 foliations. These foliations are therefore clearly recognisable only in microlithons and rootless folds wrapped by the SM foliation (**Figure 6g**).

Garnet porphyroblasts (up to 0.5 mm in size) are pre-kinematic with respect to the SM foliation. They include quartz, phengite, graphite and lozenge-shaped pseudomorphs after former lawsonite, consisting of fine-grained epidote + paragonite. These inclusions (especially graphite) locally define an internal foliation (S1), discontinuous and discordant with respect to the external SM (**Figure 6f**). Garnet is slightly zoned, with a large, quite homogeneous core, and a thin rim. Spessartine decreases from core to rim, counterbalanced by almandine and grossular, that increase toward the rim. Pyrope slightly decreases outward (core: Alm_{64-69}, Sps_{20-26}, Prp_{4-6}, Grs_{2-5}; rim: Alm_{70-74}, Sps_{11-16}, Prp_{3-4}, Grs_{8-12}), thus suggesting that garnet porphyroblasts do not completely preserve prograde zoning (**Figure 7a-b-c-f**).

Potassic white mica occurs in different generations, characterized by different microstructural sites and Si contents: (i) a phengite with high- to medium-Si contents (mostly in the range Si=3.34–3.47 a.p.f.u., with few analyses at Si=3.51-3.54 a.p.f.u.) defines the early S1 foliation still preserved in the microlithons (**Figure 6g**). As for sample VS17, it cannot be excluded that some of this phengite formed prior to the development of the S1 foliation and was then re-oriented during the D1 deformation event; however, a reliable distinction with pre-D1 related phengite generation was not possible on a microstructural basis. (ii) A low-Si muscovite (Si=3.11 – 3.27 a.p.f.u.) defines the later S2 foliation, clearly recognisable in the hinges of rootless folds wrapped by the SM mylonitic foliation (**Figure 6h**). White mica defining the SM mylonitic foliation is mostly a high-Si phengite, overlapping in composition with that defining the S1 foliation (i.e. Si=3.30–3.60 a.p.f.u.). However, the strongly transpositive nature of the SM mylonitic foliation, which reoriented both S1 and S2, make it difficult to understand whether this high-Si phengite represents a third white mica generation, grown during the T1 mylonitic event, or rather corresponds to re-oriented white mica of the first white mica generation, grown during the D1 deformation event and re-oriented during the T1 mylonitic event.

Chloritoid is abundant (~18 vol%) and mostly occurs in the micaceous domains, where it is re-oriented along the main mylonitic foliation, locally defining microfolds (**Figure 6i**). Its composition is quite homogeneous, with almost constant X_{Mg} values between 0.08 and 0.16 (**Table S1**).

Chlorite replaces garnet along its rim and fractures. It varies in composition from pycnoclorite to ripidolite. Graphite is quite abundant and is concentrated in the micaceous domains. Rutile (locally replaced by titanite), tourmaline and apatite are the other accessory minerals.

The mineral assemblages – deformation diagram (blastesis-deformation) reconstructed for this sample (**Table 2**) allows recognising four main metamorphic events (M1a to M3), each one characterized by its own equilibrium assemblage. Only the D1, D2 and D3 deformation events are directly associated with M1b, M2 and M3 metamorphic events, because S1, S2 and SM foliations do not allow preserving the older foliations. Evidence of pre-D1 deformation stage, indeed, were not observed in this sample although metamorphic relics of prograde and P-peak (M1a) conditions are preserved. The definition of the metamorphic conditions during T1 is beyond the aim of this paper and were not investigated in detail.

6. Thermobarometry

6.1 P-T pseudosections

6.1.1 Sample VS17 (metapelite)

Growth of garnet outer core (M1a event)

The growth of the inner garnet cores, strongly enriched in Mn, was not modelled through the pseudosection approach for two reasons: (i) these cores are volumetrically minor and highly scattered throughout the sample, thus suggesting that their growth was controlled by local enrichment in Mn of the bulk rock composition, rather than to the prograde P-T conditions; (ii) the garnet solution model (White et al., 2014) was calibrated for garnets with an almandine component higher than the spessartine component, and could be therefore inappropriate for garnets with an opposite behaviour, such as the inner cores of garnet in sample VS17. The pseudosection calculated using the measured bulk composition (excluding garnet inner cores) for sample VS17 (**Table 1**) was therefore used to constrain the P-T conditions for the growth of garnet outer core (M1a event; **Table 2**). The modelled pseudosection (**Figure 8a-c**) is dominated by three- to five- variant fields, with few two- and six- variant fields, and shows a relatively simple topology. Garnet, white mica and glaucophane are predicted to be stable in the whole P-T region of interest; lawsonite is stable at T < 480°C and chloritoid stability field is limited to T < 550°C. Chlorite is predicted to be completely consumed at P > 20 kbar, whereas a jadeite-rich clinopyroxene is modelled at P > 25 kbar.

The observed M1a mineral assemblage consists of Grt outer core + Ph + Cld + Rt + Lws + Gln (+Qz). Both lawsonite and glaucophane are not preserved, but their former occurrence in the M1a assemblage is testified by Ep + Pg pseudomorphs included within Grt outer core and by fine-grained aggregates of green Bt + Ab + Chl in the matrix, respectively. The vol% of each modelled phase is also reported in **Table S4**.

This M1a assemblage is modelled in a relatively wide P-T range at 20-27 kbar, 400-480°C (**Figure 8a-c**). P-T conditions for the M1a event can be more tightly constrained from the intersection of Grt outer core (average composition: $Alm_{63}Grs_4Prp_5Sps_{26}$) compositional isopleths, which cross each other in the relatively narrow P-T range of 26.5-27.5 kbar, 460-475°C, within the Grt + Ph + Cld + Lws + Gln + Jd (+Qz) field assemblage (**Figure 8c**). The modelled chloritoid compositional isopleths corresponding to the highest measured X_{Mg} values (X_{Mg} = 0.12 – 0.13) cross Grt isopleths in the same P-T range. Lower X_{Mg} values (X_{Mg} = 0.09 – 0.11) measured mostly in chloritoid cores are compatible with its prograde growth. Jadeite was not observed in the studied sample but it is predicted to occur at these P-T conditions. However, the predicted amount of jadeite is very low (1.81 vol%, see **Figure 8d** and **Table S4**) and it is likely that it was completely replaced by retrograde phases during retrogression. Due to the difficulties in attributing the measured phengite compositions to a specific phengite generation (i.e. prograde pre-D1 vs. sin-D1; see *Section 5.3.1*), the modelled phengite compositional isopleths were not used to further constrain the P-T conditions for the M1a event. Nevertheless, it is worth of note that the observed phengite compositions are predicted to be stable between 17 and 28 kbar, thus encompassing the whole prograde evolution of the studied sample. At the estimated peak-P conditions, a high-Si phengite (Si = 3.50-3.58 a.p.f.u.) is predicted to occur, which is quite in agreement with the maximum amount of Si observed in the analysed phengites (few analyses up to Si = 3.62 a.p.f.u.).

Growth of garnet rim (M1b event)

The pseudosection calculated using the fractionated bulk composition (i.e. measured bulk composition subtracted of garnet inner and outer cores), was used to constrain the P-T conditions for the growth of garnet rim, corresponding to the M1b event (**Figure 8b-d**). The topology of the fractionated pseudosection is similar to that of the unfractionated one (**Figure 8a-c**), with limited shift of the field boundaries. The observed M1b mineral assemblage consists of Grt rim + Cld + Ph + Rt + Gln (+Qz), with glaucophane and lawsonite completely re-equilibrated during the decompression (see **Table S4** for the vol% of each phase). This assemblage is modelled in a relatively narrow P-T range at 20-25 kbar, 470-530°C.

The intersection of garnet rim (average composition: $Alm_{83}Grs_6Prp_7Sps_2$) compositional isopleths (**Figure 8d**) further constrains the P-T conditions of the M1b event at 20-25 kbar, 490-520°C. The nearly parallel trend of the garnet compositional isopleths does not allow to constrain P conditions more tightly. The modelled chloritoid isopleths corresponding to the composition of chloritoid rim (X_{Mg} of 0.12 – 0.14) cross Grt isopleths in the same P-T range. Phengite composition predicted at these P-T conditions is mostly in the range Si = 3.42-3.47 a.p.f.u., thus suggesting that phengites with higher Si contents (i.e. up to Si=3.62 a.p.f.u.) belong to a pre-D1 generation, even if they are now oriented parallel to the S1 foliation.

6.1.2 Sample MOM15 (metapelite)

Growth of garnet core (M1a event)

The pseudosection for sample MOM15 (**Figure 9a-b**) was calculated in the same P-T range as that modelled for sample VS17, thus allowing direct comparison between the two metapelitic samples. As for sample VS17, the pseudosection calculated using the measured bulk composition was used to constrain P-T conditions for the growth of garnet core, corresponding to the M1a event.

The modelled pseudosection (**Figure 9a**) is dominated by three- to five- variant fields, with few six- variant fields, and shows a topology slightly different with respect to that of sample VS17. Garnet and white mica are predicted to be stable in the whole P-T region of interest, but glaucophane is limited to P < 25 kbar and T < 530°C. The relative stability of lawsonite, chloritoid, chlorite and jadeite are similar to that predicted for sample VS17, but the position of the corresponding phase-in or phase-out boundaries is slightly different. Specifically, lawsonite is stable at T < 480°C, chloritoid disappears at T > 580°C, chlorite is stable at P < 19 kbar, and low amounts of jadeite appear at P > 23 kbar. Moreover, kyanite is predicted to be stable at T > 550-580°C, depending on pressure.

The observed M1a assemblage consists of Grt core + Ph + Cld + Rt + Lws (+Qz). Lawsonite is not preserved, but its former occurrence in the M1a assemblage is testified by the Ep + Pg pseudomorphs included within garnet core. This specific assemblage do not correspond to that predicted by the pseudosection, because jadeite is always expected to coexist with the observed M1a mineral phases. However, the modelled modal amounts of jadeite in the lawsonite stability field is low (2.5 vol%, see **Figure 9b** and **Table S4**) and it is likely that this phase was completely replaced during exhumation. Considering jadeite as part of the M1a assemblage, this is predicted to be stable at P > 25 kbar and T < 480°C.

The intersection of garnet core (average composition: $Alm_{65}Grs_{4}Prp_{6}Sps_{25}$) compositional isopleths (**Figure 9b**) tightly constrains the P-T conditions for the M1a event at 26.5-28.5 kbar, 465-480°C. The modelled chloritoid compositional isopleths corresponding to the most frequent measured X_{Mg} values (X_{Mg}=0.11-0.12) cross Grt isopleths in the same P-T range. The modelled phengite compositional isopleths were not used to further constrain these P-T conditions, due to the uncertainties in the identification of different phengite generations (i.e. pre-D1 vs. syn-D1: see Section 5.3.2). However, it is worth noting that phengite composition modelled at peak-P conditions is in the range Si=3.43-3.49 a.p.f.u., in agreement with most of the measured compositions (Si up to 3.47 a.p.f.u.). The P-T conditions estimated for the M1a, peak-P, event are remarkably consistent to those obtained for the same metamorphic event from sample VS17.

6.1.3 Sample VS20 (Fe-Ti metagabbro)

Growth of garnet core (M1a event)

The pseudosection calculated using the measured bulk composition was applied to constrain P-T conditions for the growth of garnet core, corresponding to the M1a event (**Figure 10a-b**). The modelled pseudosection

(**Figure 10a**) is dominated by three- and four- variant fields, with minor five- and six- variant fields and shows a relatively simple topology, with fields that are mostly T-dependent. Omphacite and garnet are predicted to be stable in the whole P-T region of interest, and glaucophane-free assemblages are stable only at the highest P and T conditions (P > 30 kbar, T > 560°C). Lawsonite is stable at T < 550°C, chlorite is predicted to disappear at T > 470°C and quartz/coesite are limited to T > 480°C; the stability field of talc is restricted to 430-490°C for P > 26 kbar.

The observed M1a assemblage consists of Grt core + OmpIII + Gln + Tlc + Lws + Rt. Lws is not preserved but its former occurrence is testified by lozenge-shaped Ep + Pg pseudomorphs included in garnet core. OmpIII is included in garnet core and it has been therefore associated to the M1a assemblage. The vol% of each modelled phase is also reported in **Table S4**. This assemblage is modelled in the relatively narrow P-T range > 26 kbar, 430-490°C (**Figure 10b**). Compositional isopleths of Grt core (average composition: $Alm_{72}Grs_{18}Prp_5Sps_4$) and OmpIII ($Jd_{45-47}$) perfectly intersect within this field, thus constraining P-T conditions for the M1a event at 27-29.5 kbar, 460-480°C (**Figure 10b)**. The predicted modal composition at these P-T conditions is coherent with that observed in sample VS20.

Influence of Fe^{3+}: P-X(Fe_2O_3) and T-X(Fe_2O_3) pseudosections

The influence of Fe^{3+} on the calculated P-T conditions for the M1a event was explored for the VS20 sample through the calculation of isothermal (**Figure S1a**) P-X(Fe_2O_3) and isobaric (**Figure S1b**) T-X(Fe_2O_3) pseudosections. X(Fe_2O_3) corresponds to $Fe_2O_3/(Fe_2O_3+FeO)$. The P-X(Fe_2O_3) and T-X(Fe_2O_3) pseudosections were calculated at 470°C and 28 kbar, respectively, i.e. at the P-T conditions estimated for the metamorphic peak M1a in the Fe^{+3}-absent system and independently confirmed by the results of the pseudosection modelling of the metapelite samples.

Based on the stability field of the observed M1a assemblage (Grt + Omp + Gln + Tlc + Lws) as predicted by the isothermal P-X(Fe_2O_3) pseudosection (**Figure S1a**), X(Fe_2O_3) can be constrained at values lower than 0.1. For more oxidized conditions, in fact, talc is not predicted to be stable in the M1a assemblage. The increase of X(Fe_2O_3) from 0 to 0.1 would result in a slight increase of the estimated pressure conditions from 28 to 30-31 kbar. On the opposite, the modelled isobaric T-X(Fe_2O_3) pseudosection (**Figure S1b**) shows that X(Fe_2O_3) has a very minor influence on the estimated temperature conditions, which increase of less than 20°C at increasing X(Fe_2O_3). Moreover, the predicted stability field of the M1a assemblage in the T-X(Fe_2O_3) pseudosection further constrains the maximum X(Fe_2O_3) at values lower than 0.05. The modelled compositional isopleths of garnet and omphacite (**Figure S1**) converge in the modelled M1a field assemblage, further confirming that X(Fe_2O_3) values during the M1a metamorphic stage were low. Overall, the results of the T-X(Fe_2O_3) and P-X(Fe_2O_3) pseudosections show that the P-T conditions inferred from sample VS20 in the Fe^{+3}-absent system can be considered reliable and that the occurrence of minor

amounts of trivalent Fe would eventually result in a slight increase of both pressure and temperature conditions for the M1a event (i.e. ΔP = 2-3 kbar; ΔT=10-15°C).

6.3 Optimal thermobarometry

The Thermocalc "Average PT" (AvPT) method (i.e. "Optimal thermobarometry": Powell & Holland, 1994) was applied on both the M1a and M1b assemblages for the metapelites (VS17 and MOM15), and to the M1a assemblage for the metabasic sample (VS20). The compositional analysis of each phase used for the modelling are reported in **Table S2** (VS17) and **Table S3** (MOM15 and VS20). The results of the AvPT calculation are reported in **Table 3**. Various sources of uncertainty (analytical precision, thermodynamic data, activity-composition relationships; Fraser, Worley, & Sandiford, 2000; Powell, 1978, 1985; Powell & Holland, 1985) contribute to relatively large uncertainties in the final THERMOCALC estimates (e.g. 2σ uncertainties on P-T results for the studied samples are generally lesser than ±29°C and ±7 kbar).

P-T conditions of the M1a event estimated from samples MOM15 (475-485°C, 26.5-28.5 kbar; **Table 3**) and VS20 (460-470°C, 26-28 kbar; **Table 3**) are perfectly in agreement with those constrained through the pseudosection approach. The set of mineral compositions selected for sample VS17 (**Table 3**) allows constraining a prograde evolution from ca. 420°C, 21 kbar to peak conditions of ca. 480-500°C, 25-29 kbar. Although the uncertainties associated to these P-T estimates are large, the prograde evolution is quite well defined and the peak M1a conditions are consistent with those estimated from the pseudosections.

P-T conditions for the M1b event have been calculated only for metapelite samples, because the number of reactions calculated for the metabasic sample VS20 was not sufficient to converge to a result. P-T conditions of ca. 520°C, 27 kbar and 490°C, 25 kbar are suggested by samples VS17 and MOM15, respectively, with large uncertainties especially on pressure values.

Overall, the AvPT results are remarkably consistent through different chemical systems and in good agreement with the pseudosection results, although the errors on pressure are significantly larger. Combining the estimates obtained by the pseudosection approach with those of AvPT, P-T conditions for the M1a event are constrained at 25-29 kbar, 460-510°C. The M1b event is less constrained than M1a. Both the pseudosections and the AvPT data show that the M1b event occurred at higher-T and lower-P than the M1a event, thus suggesting that a slight increase in T was recorded by the IPZ, developed during a decompression stage. P-T conditions estimated for the M1b event are in the range 21-25 kbar, 500-530°C (**Table 3**).

7. Discussion

7.1 P-T evolution of the IPZ in the Susa Valley

Metamorphic conditions for the IPZ in the Susa Valley have been constrained by combining microstructural observations, mineral chemical analyses and P-T pseudosection modelling of metapelite

and Fe-Ti metagabbro samples. Four texturally distinguished mineral assemblages have been defined to testify four Alpine metamorphic stages (M1a, M1b, M2, M3) developed under different P-T conditions. The first two metamorphic events have been quantitatively constrained using the thermodynamic modelling approach, while the later re-equilibration events have been only qualitatively constrained, on the basis of their mineral assemblages. The proposed complete P-T-path is reported in **Figure 11a**.

The M1a event is well preserved by metapelites, whose eclogitic M1a assemblage consists of Cld + Grt core + Ph + Qz + Rt + Lws (now replaced by Zo + Pg pseudomorphs preserved in Grt). The M1a event is also recorded by Fe-Ti metagabbro, where a typical eclogitic mineral assemblage is well-preserved, consisting of Grt + OmpIII + Gln + Ph + Rt + minor Tlc (included in Omp) + Lws (now replaced by Zo + Pg pseudomorphs preserved in Grt). The observed M1a assemblages in both metapelites and metagabbro imply that Lws-eclogite facies conditions were reached during the M1a event. Thermodynamic modelling further constrains the P-T conditions for this event at P=25-29 kbar, T= 460–510°C, at the transition between HP and UHP conditions (**Figure 11a**).

After the M1a event, the IPZ followed a prograde-decompression path (i.e., the M1b event), which still occurred under eclogitic conditions. In the metagabbro, the M1b assemblage consists of Grt rim + OmpIII + Ktp/Gln + Ph + Lws + Rt, whereas in the metapelites it consists of Cld + Grt rim + Ph + Qz + Ep + Rt. Although the P-T conditions for the M1b event are less constrained than those of M1a, both the results of thermodynamic modelling and those of Average PT suggest that a slight T increase was recorded during decompression after the M1a event. In particular, the continuous garnet growth in metapelite VS17 during decompression, highlights a prograde decompressional heating that can be considered as a growth stage developed in the Grt-Cld-Gln stability field (**Table 2**). The P-T conditions inferred for the M1b event are in the range 21-25 kbar, 500-530°C, compatible with Ep-eclogite facies conditions (**Figure 11a**).

After the M1b event, the IPZ followed a decompressional and slightly retrograde (i.e. near isothermal) trajectory, responsible for its re-equilibration under greenschist-facies conditions (M2 event). During this event, new stable mineral assemblages developed in both metagabbro (Ab + Act + Chl + Ms + Pg + Czo + Ttn), and metapelites (Ab + Ep + Ms + Pg + Ttn + Chl + Qz).

This metamorphic event overprinted the previous M1a- and M1b-related textures and mineral assemblages, as for instance highlighted by the occurrence of lozenge-shaped pseudomorphs consisting of green Bt + Ab + Chl (±Qz) after former Gln or Jd.

The last metamorphic event is defined by the development of the M3 mineral assemblage, which consists of Hbl (Prg) + Pl (An_{20}) + Di + Bt + Ep + Ilm in metagabbro and of Ep + Bt in metapelites. These assemblages suggest that the M3 event was related to a nearly-isobaric heating following the M2 stage, at P-T conditions which reached the boundary between greenschist- and amphibolite-facies.

Overall, the P-T path inferred for the IPZ in the Susa Valley shows a clockwise-like trajectory. The prograde portion of this trajectory (i.e., subduction-related) took place along a very low geothermal

gradient (5-6 °C/km), up to the eclogitic peak-P conditions (M1a stage). This implies a burial path in the field of "cold subduction", according to the definition of Chen, Ye, Wu, & Guo, (2013). The exhumation-related path is marked by a first slight decompressional step of about 6-7 kbar down to the thermal peak (about 510 °C), developed in the Lws-absent field for the pelitic system (**Figures 8 and 9**), and marked by a slightly higher thermal gradient (ca. 8-9 °C/km), still compatible with a subduction channel environment (M1b event).

The subsequent exhumation stage is marked by a further decompression of almost 17-18 kbar, associated to a slight temperature decrease (cooling down to 470-480°C), implying an increase of the thermal gradient to about 25 °C/km, compatible with continental collision regime (M2 event). Afterwards, the IPZ continued to follow the decompressional path recording a heating (M3), and finally cools.

7.2 Comparison with previous estimates and with the P-T evolution of other IPZ meta-ophiolites

Peak metamorphic conditions inferred for the IPZ in the Susa Valley substantially confirm peak-T already defined by Pognante & Kienast (1987; peak at P>12–13 kbar, T=450–500°C) more than 30 years ago, but point to remarkably higher peak-P (ΔP= 12-15 kbar). This is the same trend already followed in the definition of peak P–T conditions for other HP units in the Western Alps, in parallel with the progressive improvement of thermodynamic modelling approaches that extended the limits of conventional thermobarometry. More recently, Agard et al. (2001) proposed P-T conditions of 18-20 kbar, 450-520°C for the eclogitic assemblage in the IPZ (i.e., Rocciavrè nappe); we interpret their eclogitic event as likely corresponding to the here described M1b event. The P-T path calculated for the Colle delle Finestre area by Agard et al. (2001), in fact, suggests the existence of a metamorphic event (not estimated in details; **Figure 11b**) at higher pressure than that estimated for the thermal peak, which lead us to assimilate their thermal-peak to our M1b event.

In the Maurienne area, to the north to the study area, Plunder et al. (2012) proposed P-T conditions for the peak eclogite-facies in the IPZ similar to those proposed in this study. Their temperature values are remarkably similar to those proposed for the Susa Valley (T~470°C vs. T=460–510°C), while P values are slightly lower (P~25 kbar vs. P=25-29 kbar), but indeed comparable within the uncertainties.

Metamorphic evolutions similar to those inferred in this study have been proposed by several authors for other units of the IPZ, both toward the north and toward the south with respect to the central portion of the Susa Valley (**Figure 11b**). For the Zermatt-Saas meta-ophiolite, Angiboust et al. (2009), Bucher et al. (2005) and Groppo et al. (2009) proposed, for the eclogite-facies peak conditions, P values similar to those obtained in this work (P~26-28 kbar), and slightly higher T values (T~500-550°C). In the Monviso meta-ophiolite Angiboust et al. (2012), Balestro et al. (2014) and Groppo & Castelli, (2010) calculated, for the eclogite-facies peak conditions, P values slightly lower with respect to those obtained in this work (P~25 kbar), and slightly higher T values (T~500-550°C).

Overall, the peak-P conditions registered by the different eclogitic meta-ophiolitic units along the Western Alpine belt can be considered as significantly comparable (within the uncertainties) with results obtained in this work (apart from the already recognized Lago di Cignana UHP unit, wherein Frezzotti et al., 2011 reported the occurrence of microdiamonds, and a portion of the Zermatt-Saas unit, wherein Luoni et al., 2018 reported similar UHP conditions in the Ti-chondrodite bearing serpentinite). This suggests that subduction of the oceanic lithosphere occurred in a relatively coherent way all along its length. Furthermore, except for the late heating event, which has never been reported in the other meta-ophiolitic units (**Figure 11a-b**), also the retrograde (exhumation-related) path shows several similarities with that of the other meta-ophiolitic units.

8. Conclusions

This study highlights that meta-ophiolitic rocks exposed in the Susa Valley were metamorphosed under P-T conditions similar to other meta-ophiolitic units of the Western Alps. Common subduction and detachment mechanisms for the entire Western Alpine meta-ophiolitic belt were already suggested by Agard et al. (2009) and Angiboust et al. (2012) on the basis of similarities in the P-T trajectories between the Zermatt-Saas ophiolite to the north and the Monviso ophiolite to the south.

The few differences in peak P-T conditions between different areas ($\Delta P \sim 5$ kbar, $\Delta T < 80°C$) might reflect local conditions, (e.g., related to local variation in composition due to fluid-rock interactions, heat flux perturbations, variation in non-lithostatic pressure field etc.) rather than actual different positions (e.g. depth) along the subduction channel.

It is remarked that the actual setting of the meta-ophiolitic units in the Western Alps is the result of late deformation processes occurred during exhumation, with disruptions along regional scale first-order tectonic contacts. However, we show that highly competent lithologies, such as Fe-Ti metagabbro, often escaped deformation during both subduction and exhumation stages, especially if they form relatively small bodies embedded within less competent lithologies. In the absence of deformation (and of a pervasive fluid circulation enhanced by deformation itself), metamorphic re-equilibration occurred statically, with frequent development of coronitic structures and preservation of abundant igneous relics (as reported in the Rocciavrè area by Pognante, 1985). This implies that equilibrium conditions were not attained neither during eclogitic metamorphism nor during retrogression; coronitic microstructures are, in fact, generally interpreted as the result of diffusion, driven by chemical potential gradients between minerals in local equilibrium domains (e.g. Schorn & Diener, 2017).

The composition of the oceanic crust (basement and metasediments) played a fundamental role in the subduction (and exhumation), as proposed by Agard, Plunder, Angiboust, Bonnet, & Ruh (2018). The IPZ in the Susa Valley mostly consists of meta-ophiolites (serpentinite, metabasite and metagabbro), whereas meta-sediments are relatively scarce (see e.g., Pognante, 1979; 1980). Considering this, the estimated peak-

P (~28 kbar) can be considered as the limit conditions from which the oceanic crustal rocks can be recovered during exhumation (Agard et al., 2018).

Comparing the exhumation history of the IPZ with the P-T trajectory proposed for the adjacent Dora Maira unit (**Figure 11c**), we propose some considerations about the coupling of these oceanic and continental crustal units. The remarkably similarities between the P-T conditions estimated for the M1b event (this work) and P-T conditions experienced by the Dora Maira unit in this sector (~20 kbar and 520 °C; syn-D1, Gasco et al., 2011), allowed us to infer that the coupling likely occurred at this stage (see **Figure 11c**). The coupling of the relatively cold IPZ oceanic unit with the likely hotter Dora Maira continental unit might also explain the slight T increase registered in the IPZ after the P-peak. This early coupling might have modified the exhumation path of the IPZ, leading to exhumation-related buoyancy forces.

It might be therefore concluded that the less dense units of the subducted continental crust were not the only and decisive trigger for the exhumation of eclogitized oceanic lithosphere, as recently suggested by Angiboust & Glodny (2020). Similar dynamics are widely reported in other subduction margins (including present-day subduction zones), such as along the circum-Pacific domain (see Agard et al., 2018 and references therein).

Acknowledgments

We thank S. Angiboust, an anonymous reviewer and P. Agard for their constructive and thorough reviews.

This work was financially supported by Ministero dell'Universita` e della Ricerca Scientifica e Tecnologica (M.I.U.R.).

References

Agard, P., Jolivet, L., & Goffe, B. (2001). Tectonometamorphic evolution of the Schistes Lustrés complex: implications for the exhumation of HP and UHP rocks in the western Alps. *Bulletin de la Société géologique de France,* 172, 617–636.

Agard, P., Monie, P., Jolivet, L., & Goffe, B. (2002). Exhumation of the Schistes Lustrés complex: in situ laser probe 40Ar/39Ar constraints and implications for the Western Alps. *Journal of Metamorphic Geology,* 20, 599-618.

Agard, P., Yamato, P., Jolivet, L., & Burov, E. (2009). Exhumation of oceanic blueschists and eclogites in subduction zones: Timing and mechanisms. *Earth-Science Reviews,* 92(1-2), 53–79.

Agard, P., Plunder, A., Angiboust, S., Bonnet, G., & Ruh, J. (2018). The subduction plate interface: Rock record and mechanical coupling (from long to short time scales). Lithos, 320–321, 537–566.

Amato, J.M., Johnson, C.M., Baumgartner, L.P., & Beard, B.L. (1999). Rapid exhumation of the Zermatt-Saas ophiolite deduced from high-precision Sm–Nd and Rb–Sr geochronology. *Earth and Planetary Science Letters*, 171, 425– 438.

Angiboust, S., Agard, P., Jolivet, L., & Beyssac, O. (2009). The Zermatt-Saas ophiolite: the largest (60-km wide) and deepest (c. 70-80km) continuous slice of oceanic lithosphere detached from a subduction zone? *Terra Nova*, 21, 171-180.

Angiboust, S., Langdon, R., Agard, P., Waters, D., & Chopin, C. (2012). Eclogitization of the Monviso ophiolite (W. Alps) and implications on subduction dynamics. *Journal of Metamorphic Geology*, 30, 37-61.

Angiboust, S., Glodny, J., Oncken, O., & Chopin, C. (2014). In search of transient subduction interfaces in the Dent Blanche–Sesia Tectonic System (W. Alps). *Lithos*, 205, 298–321.

Angiboust, S. & Glodny, J. (2020). Exhumation of eclogitic ophiolitic nappes in the W. Alps: New age data and implications for crustal wedge dynamics. *Lithos*, 356-357, 105374.

Balestro, G., Cadoppi, P., Perrone, G., & Tallone, S. (2009). Tectonic evolution along the Col del Lis-Trana Deformation Zone (internal Western Alps). *Italian Journal of Geosciences*, 128(2), 331–339.

Balestro, G., Lombardo, B., Vaggelli, G., Borghi, A., Festa, A., & Gattiglio, M. (2014) Tectonostratigraphy of the northern Monviso Meta-ophiolite Complex (Western Alps). *Italian Journal of Geosciences,* 133, 409-426.

Balestro, G., Festa, A., & Tartarotti, P. (2015). Tectonic significance of different block-in-matrix structures in exhumed convergent plate margins: examples from oceanic and continental HP rocks in Inner Western Alps (northwest Italy*). International Geology Review*, 57, 581–605.

Balestro, G., Festa, A., Borghi, A., Castelli, D., Tartarotti, P., & Gattiglio, M. (2018). Role of Late Jurassic intra-oceanic structural inheritance in the Alpine tectonic evolution of the Monviso meta-ophiolite Complex (Western Alps). *Geological Magazine,* 155(2), 233-249.

Balestro, G., Festa, A., & Dilek, Y. (2019). Structural architecture of the western alpine ophiolites, and the jurassic seafloor spreading tectonics of the alpine Tethys. *Journal of the Geological Society*, 176(5), 913-930.

Barfety, J.C., Lemoine, M., De Graciansky, P.C., Tricart, P., & Mercier, D. (1995). Notice explicative de la feuille Briançon à 1/50 000 (823). Orléans: Ed. du BRGM, *Service Géologique National*, 180 pp.

Bearth, P. (1967). Die Ophiolithe der Zone von Zermatt-Saas Fee*. Beiträge zur Geologischen Karte der Schweiz, Neue Folge*, 130 pp.

Beltrando, M., Compagnoni, R., & Lombardo, B. (2010). (Ultra-) High-pressure metamorphism and orogenesis: An Alpine perspective. *Gondwana reserch,* 18, 147-166.

Bigi, G., Castellarin, A., Coli, M., Dal Piaz, G. V., Sartori, R., Scandone, P., & Vai, G. B. (1990). Structural Model of Italy, Sheets 1–2. *CNR, Progetto Finalizzato Geodinamica, SELCA Firenze*.

Borghi, A., Cadoppi, P., Porro, A., & Sacchi, R. (1985). Metamorphism in the North part of the Dora Maira Massif (Cottian Alps). *Bollettino del Museo Regionale di Scienze Naturali*, 3, 369-380.

Bousquet, R., Oberhänsli, R., Goffé, B., Wiederkehr, M., Koller, F., Schmid, S. M., Schuster, R., Engi, M., Berger, A., & Martinotti, G. (2008). Metamorphism of metasediments in the scale of an orogen: A key to the Tertiary geodynamic evolution of the Alps. In: S. Siegesmund, B. Fügenschuh, & N. Froitzheim (Eds.), *Tectonic Aspects of the Alpine-Dinaride-Carpathian System*: *Geological Society, London, Special Publications*, 298, 393-412.

Bowtell, S.A., Cliff, R.A., & Barnicoat, A. C. (1994). Sm-Nd isotopic evidence on the age of eclogitization in the Zermatt-Saas ophiolite. *Journal of Metamorphic Geology,* 12, 187–96.

Bucher, K., Fazis, Y., De Capitani, C., & Grapes, R. (2005). Blueschists, eclogites, and decompression assemblages of the Zermatt–Saas ophiolite: high-pressure metamorphism of subducted Tethys lithosphere. *American Mineralogist*, 90, 821–835.

Butler, J. P., Beaumont, C., & Jamieson, R. A. (2013). The Alps 1: A working geodynamic model for burial and exhumation of (ultra) high-pressure rocks in Alpine-type orogens. *Earth and Planetary Science Letters*, 377, 114–131.

Caby, R. (1981). Le Mésozoïque de la zone du Combin en Val d'Aoste (Alpes graies): imbrications tectoniques entre séries issues des domaines pennique, austroalpin et océanique. *Géologie Alpine* 57, 5–13.

Cadoppi, P., Carraro, F., Castelletto, M., Sacchi, R., Baggio, P., Giraud, V., & Bellardone, G. (2002). Note llustrative della carta geologica d'Italia alla scala 1:50.000, Foglio 154 Susa. *Servizio Geologico d'Italia,* pp. 123.

Cartwright, I., & Barnicoat, A. C. (2002). Petrology, geochronology, and tectonics of shear zones in the Zermatt–Saas and Combin zones of the Western Alps. *Journal of Metamorphic Geology*, 20, 263-281.

Chen, Y., Ye, K., Wu, T. F. & Guo, S. (2013). Exhumation of oceanic eclogites: thermodynamic constraints on pressure, temperature, bulk composition and density. *Journal of Metamorphic Geology,* 31, 549-570.

Chopin, C., Henry, C., & Michard, A. (1991). Geology and petrology of the coesite-bearing terrain, Dora Maira massif, Western Alps. *European Journal of Mineraology,* 3, 263-291.

Cliff, R.A., Barnicoat, A.C., & Inger, S. (1998). Early Tertiary eclogite facies metamorphism in the Monviso Ophiolite. *Journal of Metamorphic Geology*, 16, 447– 455.

Connolly, J. A. D. (1990). Multivariable phase diagrams: an algorithm based on generalized thermodynamics. *American Journal of Science,* 290, 666–718.

Connolly, J. A. D. (2005). Computation of phase equilibria by linear programming: A tool for geodynamic modeling and its application to subduction zone decarbonation. *Earth and Planetary Science Letters,* 236, 524-541.

Connolly, J. A. D. (2009). The geodynamic equation of state: what and how. *Geochemistry, Geophysics, Geosystems,* 10(10), Q10014.

Dal Piaz, G., Cortiana, G., Del Moro, A., Martin, S., Pennacchioni, G., & Tartarotti, P. (2001). Tertiary age and paleostructural inferences of the eclogitic imprint in the Austroalpine outliers and Zermatt–Saas ophiolite, western Alps. *International Journal of Earth Sciences*, 90(3), 668–684.

Dal Piaz, G. V., Bistacchi, A., & Massironi, M. (2003). Geological outline of the Alps. *Episodes,* 26, 175-180.

Deville, E., Fudral, S., Lagabrielle, Y., Marthaler, M., & Sartori, M. (1992). From oceanic closure to continental collision: A synthesis of the "Schistes lustrés" metamorphic complex of the Western Alps. *Geological Society of America Bullettin, 104*(2), 127-139.

Duchêne, S., Blichert-Toft, J., Luais, B., Télouk, P., Lardeaux, J.M., & Albarède, F. (1997). The Lu-Hf dating of garnets and the ages of the Alpine high-pressure metamorphism. *Nature*, 387, 586–9.

Elter, G. (1971). Schistes Lustrés et ophiolites de la zone piémontaise entre Orco et Doire Baltée (Alpes Graies). Hypothèses sur l'origine des ophiolites. *Géologie Alpine, Grenoble*, 47, 147-169.

Ernst, W., & Dal Piaz, G. V. (1978). Mineral parageneses of eclogitic rocks and related mafic schists of the Piemonte ophiolite nappe, Breuil-St. Jacques area, Italian Western Alps. *American Mineralogist*, 63, 621–640.

Federico, L., Capponi, G., Crispini, L., Scambelluri, M. & Villa, I. M. (2005). $^{39}Ar/^{40}Ar$ dating of high-pressure rocks from the Ligurian Alps: evidence for a continuous subduction–exhumation cycle. *Earth and Planetary Science Letters*, 240(3), 668–80.

Festa, A., Balestro, G., Dilek, Y., & Tartarotti, P. (2015). A jurassic oceanic core complex in the high-pressure monviso ophiolite (western alps, NW Italy). *Lithosphere*, 7(6), 646-652.

Fraser, G., Worley, B., & Sandiford, M. (2000). High-precision geothermobarometry across the High Himalayan metamorphic sequence, Langtang Valley, Nepal. *Journal of Metamorphic Geology,* 18, 665–681.

Frezzotti, M.L., Selverstone, J., Sharp, Z.D., & Compagnoni, R. (2011). Carbonate dissolution during subduction revealedby diamond-bearing rocks from the Alps. *Nature Geoscience*, 4, 703–706.

Fudral, S., Deville, E., Nicoud, G., Pognante, U., Guillot, P. L., Jaillard, E., de Mestre, J. E., & Toury-Lerouge, A. (1994), Notice explicative: Carte géologique de la France (1/50,000), feuille Lanslebourg-Mont d'Ambin (776), *Bur. de Rech. Geol. et Min.,* Orléans, France.

Fudral, S. (1998). Etude Geologique de la suture tethysienne dans les Alpes franco-italiennes nord-occidentales de la Doire Ripaire (Italie) a la region de Bourg Sint Maurice (France). *Ph.D. dissertation, University of Grenoble, France*, 305 pp.

Fuhrman, M. L., & Lindsley, D. H. (1988). Ternary-feldspar modeling and thermometry. *American Mineralogist*, 73, 201-15.

Gasco, I., Gattiglio, M., & Borghi, A. (2011). Lithostratigraphic setting and P–T metamorphic evolution for the Dora Maira Massif along the Piedmont Zone boundary (middle Susa Valley, NW Alps). *International Journal of Earth Sciences*, 100, 1065–1085.

Gasco, I., Gattiglio, M. & Borghi, A. (2013). Review of metamorphic and kinematic data from Internal Crystalline Massifs (Western Alps): PTt paths and exhumation history. *Journal of Geodynamics*, 63, 1– 19.

Ghignone, S., & Gattiglio, M. (2013). Late to post-metamorphic cross-section trough the Piedmont Zone in the lower Susa Valley (Western Alps). *Rendiconti OnLine della Società Geologica Italiana*, 29, 66-69.

Ghignone, S., Gattiglio, M., Balestro, G., & Borghi, A. (2020) Geology of the Susa Shear Zone (Susa Valley, Western Alps). *Journal of maps*, 16(2), 79-86, https://doi.org/10.1080/17445647.2019.1698473 .

Green, E. C. R., Holland, T. J. B. & Powell, R. (2007). An order-disorder model for omphacitic pyroxenes in the system jadeite-diopside-hedenbergite-acmite, with applications to eclogite rocks. *American Mineralogist*, 92, 1181–1189.

Green, E. C. R., White, R. W., Diener, J. F. A., Powell, R., Holland, T. J. B. & Palin, R. M. (2016). Activity–composition relations for the calculation of partial melting equilibria in metabasic rocks. *Journal of Metamorphic Geology*, 34, 845–869.

Groppo, C., & Castelli, D. (2010). Prograde P-T evolution of a lawsonite eclogite from the Monviso meta-ophiolite (Western Alps): Dehydration and redox reactions during subduction of oceanic FeTi-oxide gabbro. *Journal of Petrology,* 51, 2489-2514.

Groppo, C., Beltrando, M., & Compagnoni, R. (2009). The P-T path of the ultra-high pressure Lago Di Cignana and adjoining high-pressure meta-ophiolitic units: Insights into the evolution of the subducting Tethyan slab. *Journal of Metamorphic Geology,* 27, 207-231.

Groppo, C., Ferrando, S., Gilio, M., Botta, S., Nosenzo, F., Balestro, G., Festa, A., & Rolfo, F. (2019). What's in the sandwich? New P–T constraints for the (U) HP nappe stack of southern Dora-Maira Massif (Western Alps). *European Journal of Mineralogy, 31*(4), 665–683.

Holland, T. J. B. & Powell, R. (1998). An internally consistent thermodynamic data set for phases of petrologic interest. *Journal of Metamorphic Geology*, 16, 309–343.

Holland, T. J. B. & Powell, R. (2011). An improved and extended internally consistent thermodynamic dataset for phases of petrological interest, involving a new equation of state for solids. *Journal of Metamorphic Geology*, 29, 333–383.

Lagabrielle Y., Polino R., Auzende J. M., Blanchet R., Caby R., Fudral S., Lemoine M., Mevel C., Ohnestetter M., Robert D., & Tricart P. (1984). Les témoins d'une tectonique intraocéanique dans le domaine téthysien: analyse du rapport entre les ophiolites et leur couvertures métasédimentaires dans la zone piémontaise des Alpes franco-italiennes. *Ofioliti*, 9, 67-88.

Leardi, L., & Rossetti, P. (1985). Caratteri geologici e petrografici delle metaofioliti della Val d'Ala (valli di Lanzo, Alpi Graie*). Bollettino dell'Associazione Mineraria Subalpina*, 22, 421-441.

Lemoine, M., & Tricart, P. (1986). Les Schistes lustrés des Alpes occidentales: Approche stratigraphique, structurale et sedimentologique. *Eclogae Geologicae Helvetiae*, 79, 271–294.

Locatelli, M., Verlaguet, A., Agard, P., Federico, L., & Angiboust, S. (2018). Intermediate-depth brecciation along the subduction plate interface (Monviso eclogite, W. Alps). *Lithos,* 320-321, 378-402.

Locatelli, M., Federico, L., Agard, P., & Verlaguet, A. (2019). Geology of the southern Monviso metaophiolite complex (W-Alps, Italy). *Journal of Maps,* 15 (2-3), 283-297.

Lombardo, B., Nervo, R., Compagnoni, R., Messiga, B., Kienast, J., Mevel, C., Fiora, L., Piccardo, G., & Lanza, R. (1978). Osservazioni preliminari sulle ofioliti metamorfiche del Monviso (Alpi Occidentali). *Rendiconti Societa` Italiana di Mineralogia e Petrologia*, 34, 253–305.

Lombardo, B., & Pognante, U. (1982). Tectonic implications in the evolution of the Western Alps ophiolite metagabbros. *Ofioliti*, 2, 371-394.

Luoni, P., Rebay, G., Spalla, M. I., & Zanoni, D. (2018). UHP Ti-chondrodite in the Zermatt-Saas serpentinite: Constraints on a new tectonic scenario. *American Mineralogist, 103*(6), 1002–1005.

Manzotti, P., Ballèvre, M., Zucali, M., Robyr, M., & Engi, M. (2014). The tectonometamorphic evolution of the Sesia-Dent Blanche nappes (internal Western Alps): review and synthesis. *Swiss Journal of Geosciences*, 107, 309-336.

Martin S., Tartarotti P., & Dal Piaz G. V. (1994). The Mesozoic ophiolites of the Alps: a review. *Bollettino di Geofisica Teorica e Applicata, 36*, 175-216.

Michard, A., Avigad, D., Goffé, B., & Chopin, C. (2003) The high-pressure metamorphic front of the south Western Alps (Ubaye-Maira transect, France, Italy). *Schweizerische Mineralogische und Petrographische Mitteilungen,* 84, 215–235.

Monié, P. & Philippot, P. (1989). Mise en évidence de l'âge éocène moyen du métamorphisme de haute-pression dans la nappe ophiolitique du Monviso (Alpes occidentales) par la méthode ^{39}Ar-^{40}Ar. *Comptes rendus de l'Académie des sciences. Série 2, Mécanique, Physique, Chimie, Sciences de l'univers, Sciences de la Terre,* 309(2), 245–51.

Morimoto, N. (1988). Nomenclature of Pyroxenes. *Mineralogy and Petrology,* 73, 1123-1133.

Negro, F., Bousquet, R., Vils, F., Pellet, C.-M., & Hänggi-Schaub, J. (2013). Thermal structure and metamorphic evolution of the Piemont-Ligurian metasediments in the northern Western Alps. *Swiss Journal of Geosciences,* 106, 63-78.

Nicolas, A. (1967). Geologie des Alpes piemontaises entre Dora Maira et Grand Paradis. *Travaux du Laboratoire de Geoligue de la Faculté des Sciences de l'Université de Grenoble*, 43, 139-167.

Plunder, A., Agard, P., Dubacq, B., Chopin, C., & Bellanger, M. (2012). How continuous and precise is the record of P-T paths? Insights from combined thermobarometry and thermodynamic modelling into subduction dynamics (Schistes Lustrés, W. Alps). *Journal of Metamorphic Geology,* 30(3), 323–346. doi:10.1111/j.1525-1314.2011.00969.x

Polino, R., Dela Pierre, F., Borghi, A., Carraro, F., Fioraso, G., & Giardino, M. (2002). Note illustrative della Carta Geologica d'Italia alla scala 1:50.000, Foglio 153 Bardonecchia. *Servizio Geologico d'Italia*, pp. 128.

Pognante, U. (1979). The orsiera-rocciavrè metaophiolitic complex (Italian Western Alps). *Ofioliti,* 4, 183-198.

Pognante, U. (1980) Preliminary data on the Piemonte ophiolite nappe in the lower Val Susa-Val Chisone area, Italian Western Alps. *Ofioliti,* 5, 221–240.

Pognante, U. (1984). Eclogitic versus blueschist metamorphism in the internal western alps along the susa valley traverse. *Sciences Geologiques - Bullettin,* 37, 29-36.

Pognante, U. (1985). Coronitic reactions and ductile shear zones in eclogitised ophiolite metagabbro, Western Alps, North Italy. *Chemical Geology,* 50, 99-109.

Pognante, U., & Kienast, J.R. (1987). Blueschist and Eclogite Transformations in Fe-Ti Gabbros: A Case from the Western Alps Ophiolites. *Journal of Petrology,* 28, 271-292.

Pouchou, J. L., & Pichoir, F. (1988). Determination of mass absorption coefficients for soft Xrays by use of the electron microprobe. In: D. E. Newbury (Eds.), Microbeam Analysis. San Francisco Press, San Francisco, CA, pp. 319–324.

Powell, R. (1978). Equilibrium thermodynamics in petrology. An introduction. London: Harper & Row. 284 pp.

Powell, R. (1985). Regression diagnostics and robust regression in geothermometer/geobarometer calibration: The garnet-clinopyroxene geothermometer revisited. *Journal of Metamorphic Geology*, 3, 231– 243.

Powell, R., & Holland, T. J. B. (1985). An internally consistent thermodynamic dataset with uncertainties and correlations: 1. Methods and a worked example. *Journal of Metamorphic Geology*, 3, 327-342.

Powell, R., & Holland, T. J. B. (1994). Optimal geothermometry and geobarometry. *American Mineralogist,* 79, 120–133.

Reddy, S. M., Wheeler, J., & Cliff, R. A. (1999). The geometry and timing of orogenic extension: an example from the Western Italian Alps. *Journal of Metamorphic Geology*, 17, 573–589.

Reinecke, T. (1991). Very-high-pressure metamorphism and uplift of coesite bearing metasediments from the Zermatt-Saas zone, Western Alps. *European Journal of Mineralogy*, 3, 7–17.

Reinecke, T. (1998). Prograde high- to ultrahigh-pressure metamorphism and exhumation of oceanic sediments at Lago di Cignana, Zermatt-Saas Zone, Western Alps. *Lithos,* 42, 147-189.

Ricou L. E., & Siddans A. W. B. (1986). Collision tectonics in the Western Alps. In M. P. Coward & A. C. Ries (Eds.), *Collision Tectonics, Geological Society, London, Special Publications*, 19, 229–244.

Rosenbaum, G., & Lister, G. S. (2005). The Western Alps from the Jurassic to Oligocene: spatio-temporal constraints and evolutionary reconstructions. *Earth Science Reviews*, 69, 281–306.

Rubatto, D. & Hermann, J. (2003). Zircon formation during fluid circulation in eclogites (Monviso, Western Alps): implications for Zr and Hf budget in subduction zones. *Geochimica et Cosmochimica Acta,* 67, 2173–2187.

Rubatto, D., Gebauer, D. & Fanning, M. (1998). Jurassic formation and Eocene subduction of the Zermatt-Saas-Fee ophiolites: implications for the geodynamic evolution of the Central and Western Alps. *Contributions to Mineralogy and Petrology*, 132, 269–87.

Sandrone, R., & Borghi, A. (1992). Zoned garnets in the Northern Dora - Maira Massif and their contribution to the reconstruction of its metamorphic evolution. *European Journal of Mineralogy*, 4, 465-474.

Sandrone, R., Cadoppi, P., Sacchi, R., & Vialon, P. (1993). The Dora-Maira massif. In J. F. von Raumer, & F. Neubauer (Eds.), *Pre-Mesozoic Geology in the Alps: Berlin: Springer-Verlag*, 317–325.

Schmid, S. M., Kissling, E., Diehl, T., van Hinsbergen, D. J. J., & Molli, G. (2017). Ivrea mantle wedge, arc of the Western Alps, and kinematic evolution of the Alps–Apennines orogenic system. *Swiss Journal of Geosciences*, 110, 581-612.

Schwartz, S., Tricart, P., Lardeaux, J. M., Guillot, S., & Vidal, O. (2009). Late tectonic and metamorphic evolution of the Piedmont accretionary wedge (Queyras Schistes lustrés, Western Alps): evidences for tilting during Alpine collision. *Geological Society of America Bulletin*, 121, 502–518.

Schorn, S. & Diener, J. F. A. (2017). Details of the gabbro-to-eclogite transition determined from microtextures and calculated chemical potential relationships. *Journal of Metamorphic Geology*, 35, 55–75.

Smye, A. J., Greenwood, L., & Holland, T. J. B. (2011). Garnet–chloritoid–kyanite assemblages: Eclogite facies indicators of subduction constraints in orogenic belts. *Journal of Metamorphic Geology,* 28, 753-768.

Tartarotti, P., Festa, A., Benciolini, L., & Balestro, G. (2017). Record of Jurassic mass transport processes through the orogenic cycle: Understanding chaotic rock units in the high-pressure Zermatt-Saas ophiolite (Western Alps). *Lithosphere,* 9, 399-407.

Tricart, P., & Schwartz, S. (2006). A north-south section across the Queyras Schistes lustrès (Piedmont zone, Western Alps): syn-collision refolding of a subduction wedge. *Eclogae Geologicae Helvetiae,* 99, 429–442.

Vissers, R. L. M., Van Hinsbergen, D. J. J., Meijer, P. TH., & Piccardo, G. B. (2013). Kinematics of Jurassic ultraslow spreading in the Piemonte Ligurian ocean. *Earth and Planetary Science Letters*, 380, 138–50.

Weber, S., Sandmann, S., Miladinova, I., Fonseca, R. O. C., Froitzheim, N., Münker, C., & Bucher, K. (2015). Dating the initiation of Piemonte-Liguria Ocean subduction: Lu–Hf garnet chronometry of eclogites from the Theodul Glacier Unit (Zermatt-Saas zone, Switzerland). *Swiss Journal of Geosciences*, 108, 183–199.

White, R. W., Powell, R., Holland, T. J. B., Johnson, T. E. & Green, E. C. R. (2014). New mineral activity-composition relations for thermodynamic calculations in metapelitic systems. *Journal of Metamorphic Geology,* 32, 261-286.

Whitney, D. L., & Evans, B. W. (2010). Abbreviations for names of rock-forming minerals. *American Mineralogist*, 95, 185–187.

Captions (Figures and Tables)

Figure 1: Simplified tectonic sketch-map of the Western Alps, modified after Balestro, Festa, & Tartarotti (2015) and Ghignone, Gattiglio, Balestro, & Borghi (2020). Red square indicates the study area.

Figure 2: (a) Simplified geological map of the Susa Valley, modified after Bigi et al. (1990); Fudral, (1998); Polino et al. (2002); Cadoppi et al. (2002); Balestro et al. (2009). Coloros and acronyms: Dora Maira (DM, light purple), Internal Piedmont Zone (IPZ: metaophiolites, dark green; metasedimentary cover, pale green), External Piedmont Zone (EPZ: metaophiolites, blue; metasedimentary cover, light blue), Ambin Massif (Am, pale orange). White represent the simplified alluvial quaternary cover. (b) Simplified geological cross-section through the Susa Valley, showing the geometrical relationships between different tectonic units. Stars indicate the location of the studied samples.

Figure 3: Meso-scale images, main lithologies relationships and structures from the study area: (a, b) Fe-Ti metagabbro and (a) its geometrical relationships with the host serpentinite (pen as scale). (c) Basement-cover transition, marked by a Grt-micaschist layer wrapping the lower metabasite (reverse polarity in the image). (d) D1- and D2-related folds interference relationships in calcschist-micaschist multilayer. (e) SM mylonitic foliation in Grt-Cld micaschist. (f) Superposition of the two mylonitic events: T1-related kinematic indicators (tectonic blocks wrapped by SM foliation in dashed white) crosscut by T2-related kinematic indicators (discrete shear planes in black).

Figure 4: SEM-EDS entire thin section multispectral maps, performed on (a) VS20, (b) VS17 and (c) MOM15 samples.

Figure 5: Representative microstructures of sample VS20: (a) mm-sized Grt full of inclusions; (b) Ep + Pg pseudomorphs after Lws included in Grt; (c) microstructural relationships between different Omp generations, highlighting a rim constituted by Omp III around Omp I + Omp II core; (d) patchy zoning of Omp I and Omp II; (e) Tlc inclusion in Omp; (f) symplectite (Act + Ab) around Omp and Gln; (g) microstructural relationships between different Amp generations. (a,b,d,e,f: back-scattered electron image, BSE; c,g: Plane Polarized Light, PPL).

Figure 6: Representative microstructures of samples VS17 (a-e) and MOM15 (f-i): (a) Pre-kinematic mm-sized Grt porphyroblasts; (b) lozenge-shaped Bt+Chl pseudomorph after original Gln; (c) Ep + Pg pseudomorphs after Lws included in Grt; (d) geometrical relationships between different foliation generations: S1 relics wrapped by S2 main foliation; (e) Cld inclusions in Grt. (f) S1 relics trapped inside Grt; (g) geometrical relationships between different foliation generations in Wm-rich domain; (h) microstructural relationships between S1 and S2 foliation in rootless fold preserved and wrapped by SM foliation; (i) Cld-rich layer deformed by D2-related isoclinal fold. (a,d,f,i, PPL; b,c,e,g,h: BSE).

Figure 7: Mineral Chemistry of the selected samples. (a-c): Garnet compositions plotted in the Alm, Sps, Prp diagram (a), Sps, Prp, Grs+Adr diagram (b) and Alm, Sps, Grs+Adr diagram (c); (d-f): compositional profile across representative garnet crystals, for VS20 (d), VS17 (e) and MOM15 (f) samples, respectively; (g): Q-Jd-Acm classification diagram after Morimoto (1988) for Cpx of VS20 sample; (h) Al IV vs Na classification diagram for Amp of VS20 sample; (i) Si vs Altot diagram for white micas of VS17 and MOM15 samples.

Figure 8: (a) P-T pseudosection modelled for sample VS17 using the measured bulk composition (Table 1) to constrain the P-T conditions for the growth of Grt outer core (M1a event). (b) P-T pseudosection modelled for sample VS17 using the effective bulk composition after fractionation of garnet core and used to constrain the P-T conditions for the growth of Grt rim (M1b event). Phengite-muscovite were distinguished in the pseudosections based on the Si content on 3.30 apfu. (c) Same pseudosection as in (a), contoured for Grt outer core and Cld (X_{Mg}) compositions. Black ellipse constrains the P-T conditions for the M1a event, based on the intersection of garnet outer core compositional isopleths. (d) Same pseudosection as in (b) contoured for Grt rim and Cld (X_{Mg}) compositions. Black ellipse constrains the P-T conditions for the M1b event, based on the intersection of garnet rim compositional isopleths.

Figure 9: (a) P-T pseudosection modelled for sample MOM15 using the measured bulk composition (Table 1) to constrain the P-T conditions for the growth of Grt core (M1a event). Phengite-muscovite were distinguisheded in the pseudosections based on the Si content on 3.30 apfu. (b) Same pseudosection as in (a) contoured for Grt core and Cld (X_{Mg}) compositions. Black ellipse constrains the P-T conditions for the M1a event as inferred from the intersection of garnet rim compositional isopleths.

Figure 10: (a) P-T pseudosection modelled for sample VS20 using the measured bulk composition (Table 1) to constrain the P-T conditions for the growth of Grt core (M1a event). (b) Same pseudosection as (a) contoured for Grt core and omphacite compositions. Black ellipse constrains the P-T conditions for the M1a event, as inferred from the intersection of garnet and omphacite compositional isopleths.

Figure 11: (a) P-T path calculated for the IPZ, plotted on metamorphic facies grid (modified after from Bousquet et al. (2008) and Manzotti, Ballèvre, Zucali, Robyr, & Engi, 2014; GS: greenschist facies, AM: amphibolitic facies, GRA: granulitic facies, BS: blueschist facies, ECL: eclogite facies, UHP: ultra-high pressure facies); the main tectonic gradients are also shown. Dashed blue and light blue ellipse show the results from the pseudosections and the Average PT calculations (with errors) for each sample (labelled). (b) Comparison between the P-T path inferred for the IPZ in this study and P-T paths for adjacent oceanic units and (c) the adjacent Dora Maira unit, selected from the literature.

Table 1: Effective bulk compositions (wt%) used to calculate the different pseudosections for the IPZ samples. For each sample are reported the GPS coordinates.

Table 2: Mineral abundances and relationships between the metamorphic evolution and the deformation stages of the Fe-Ti metagabbro (VS20 sample) and metapelites (VS17 and MOM15 samples). Grt InnC: garnet inner core; Grt OutC: garnet outer core; Grt R: garnet rim.

Table 3: Results of THERMOCALC Average PT calculations.

Table 1

	GPS coordinates		SiO_2	Al_2O_3	FeO	MnO	MgO	CaO	Na_2O	K_2O	tot
VS17	7°4'45"E, 45°8'43"N	*MBC*	76.08	10.52	4.53	0.11	4.14	0.14	0.8	3.69	100
		MBC-GrtC	76.35	10.49	4.32	0.05	4.15	0.12	0.8	3.72	100
MOM15	7°7'10"E, 45°10'28"N	*MBC*	57.73	20.63	12.42	0.51	3.88	0.12	0.47	4.24	100
VS20	7°16'54"E, 45°8'17"N	*MBC*	54.1	9.85	12.89	0.44	8.53	9.68	4.5	-	99.99

MBC = measured bulk composition; MBC-GrtC = effective bulk composition after fractionation of GrtC

Table 2

Deformation event				*Pre-D1*	*D1*	*D2*	*T1*	*D3/D4*
Foliation					S1	S2	SM	
	Minerals	Mode (vol %)	**Prograde relics**	**M1a ECL (P-peak)**	**M1b ECL (T-peak)**	**M2 GS**		**M3 GS/AMP transition**
VS17 Metapelite	**Qz**	35-40%	----	----	----	----	MMF conditions not reported	----
	Cld	<1%	----	----	----			
	Wm	37-43%	-Ph-	-Ph-	-Ph-	-Ms-		
	Grt	2-3%	-Grt InnC-	-Grt OutC-	-Grt R-			
	Amp	?	-Gln (?)-	-Gln-	-Gln-			
	Lws	?	----	----				
	Ep	1-2%			-Zo-	-Ep-		-Ep-
	Pg	1-3%				----		
	Bt	4-5%				-green Bt-		----
	Ti-phases	<1%	-Rt-	-Rt-	-Rt-	-Ttn-		
	Pl	4-5%				-Ab-		
	Chl	3-4%				-Rp+Pc-		
MOM15 Metapelite	**Qz**	12-15%	----	----	----	----	MMF conditions not reported	----
	Cld	15-17%	----	----	----			
	Grt	3-4%		-Grt C-	-Grt R-			
	Lws	?	----	----				
	Wm	43-47%	-Ph-	-Ph-	-Ph-	-Mus-		
	Ep	<1%			-Zo-	-Ep-		
	Pg	1-2%				----		
	Ti-phases	<1%	-Rt-	-Rt-	-Rt-	-Ttn-		
	Chl	10-12%				-Rp+Pc-		
V S	**Qz**	<1%	----	----	----	----	–	----

	Px	10-15%	-Omp I+II-	-Omp III-	-Omp III-			
	Grt	10-12%		-Grt C-	-Grt R-			
	Amp	30-35%		-Gln-	-Gln/Ktp-	-Act-		-Hbl-
	Ep	15-20%				-Czo-		-Ep-
	Pg	<1%				----		
	Tlc	<1%	----	----				
	Lws	?	----	----	----			
	Ti-phases	5-6%		-Rt-	-Rt-	-Ttn-		
	Pl	3-4%				-Ab-		-An20-
	Chl	5-7%			-	-Rp+Pc-		

Table 3

Sample	*MMF event*	*ID Calc*	*Assemblage*	*T (°C)*	*P (kbar)*	*Reactions*	*Sigfit*
VS17	M1a	1a	GrtC1+Ph1+Cld1+Lws	420±18	21.3±2.2	4	0.89
		1b	GrtC2+Ph1+Cld1+Lws	447±21	23.9±3.0	4	1.32
		1c	GrtC3+Ph1+Cld1+Lws	482±17	25.2±2.6	4	1.22
		1d	GrtC4+Ph1+Cld1+Lws	520±22	28.7±3.6	4	1.58
	M1b	2a	GrtR1+Ph2+Cld1+Lws	528±24	26.9±3.6	4	1.65
		2b	GrtR2+Ph2+Cld2+Lws	523±26	27.3±3.9	4	1.79
MOM15	M1a	3a	GrtC+Ph1+Cld1+Lws	485±12	28.1±2.2	5	0.83
		3b	GrtC+Ph1+Cld2+Lws	471±12	27.0±2.2	5	0.98
	M1b	4a	GrtR+Ph2+Cld1+Lws	500±23	25.3±3.5	4	1.69
		4b	GrtR+Ph2+Cld2+Lws	481±13	23.7±2.0	5	0.73
VS20	M1a	5a	GrtC1+OmpIII1+Tlc1+Lws	464±21	27.5±6.9	4	0.62
		5b	GrtC1+OmpIII1+Tlc2+Gln+Lws	467±29	25.5±6.6	7	2.19
		5c	GrtC2+OmpIII2+Tlc1+Lws	449±20	26.5±5.8	3	0.01

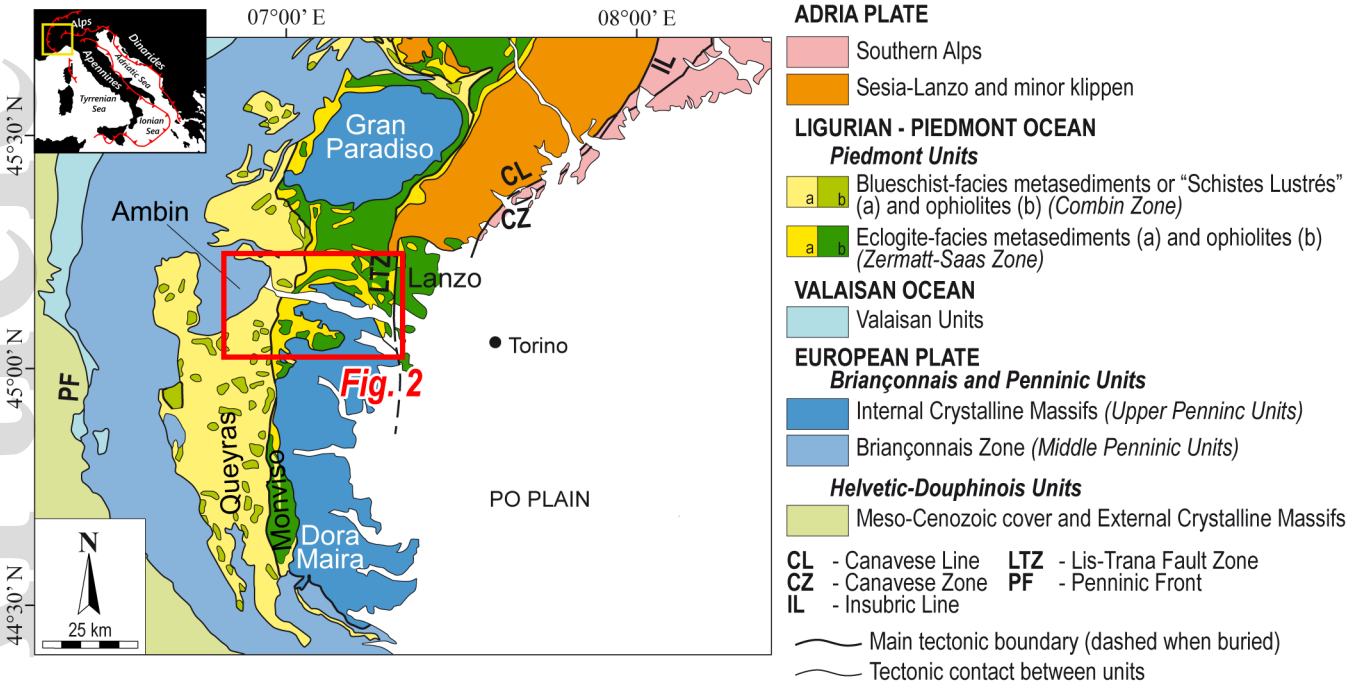

jmg_12574_f1.png

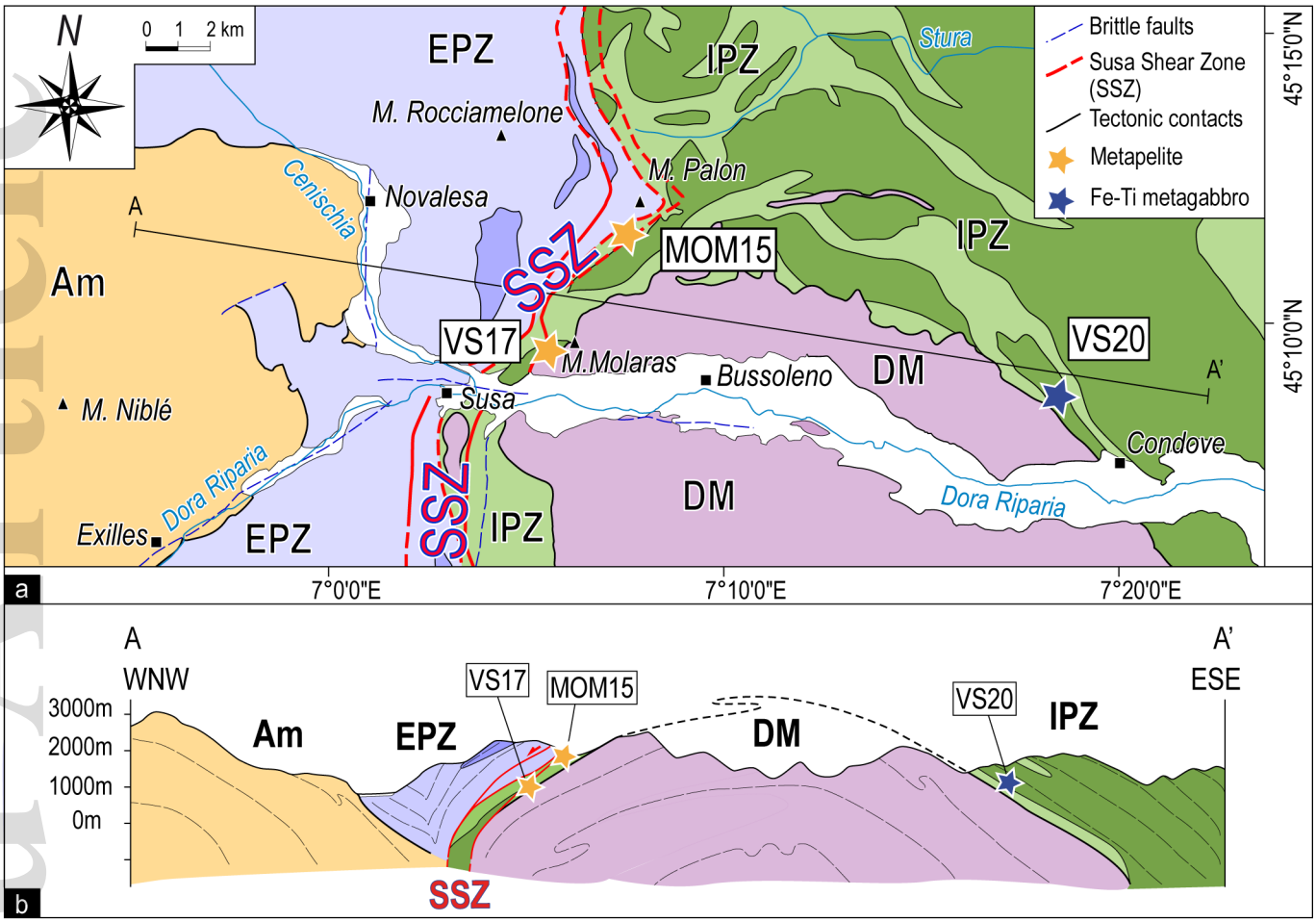

jmg_12574_f2.png

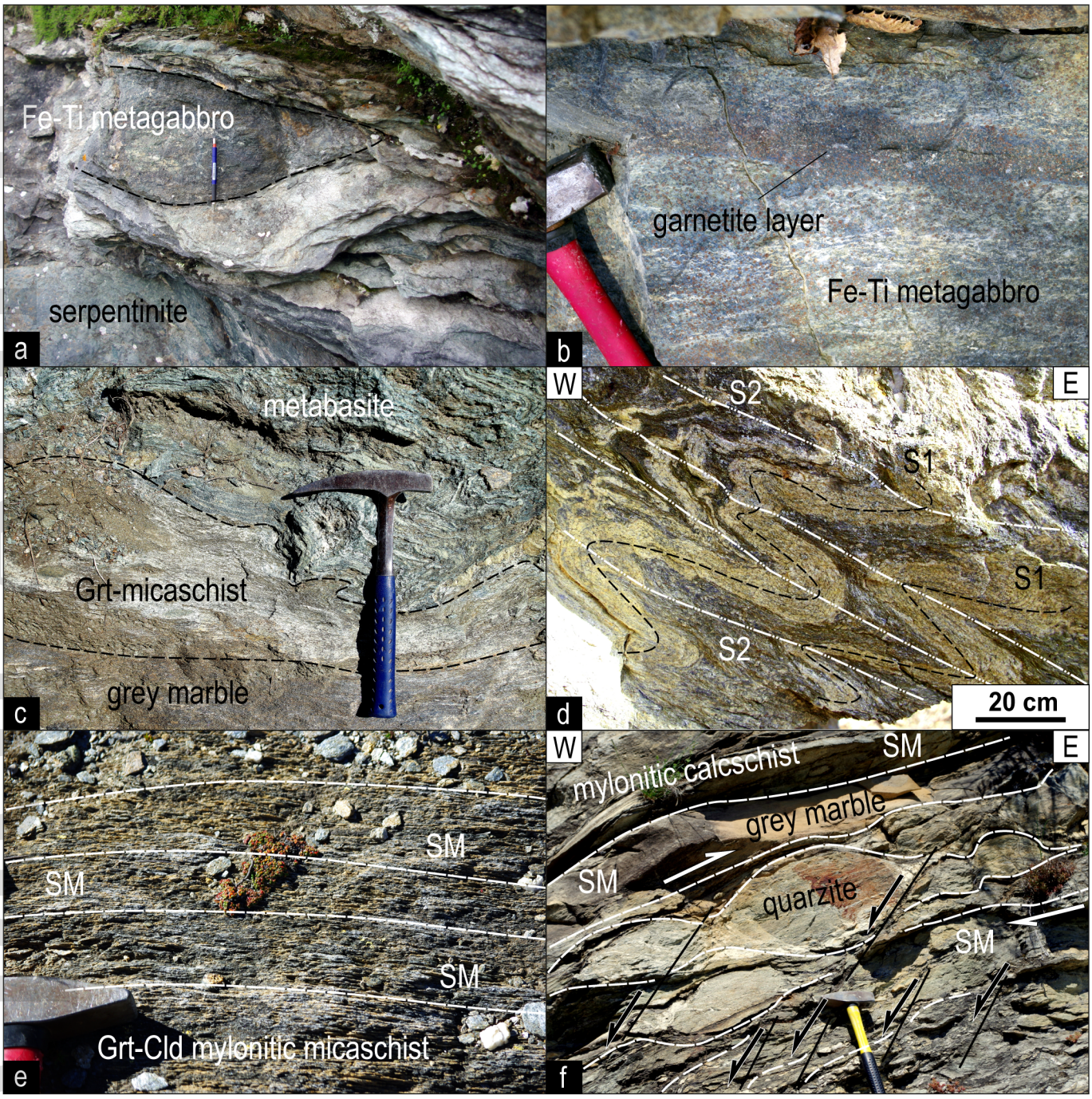

jmg_12574_f3.png

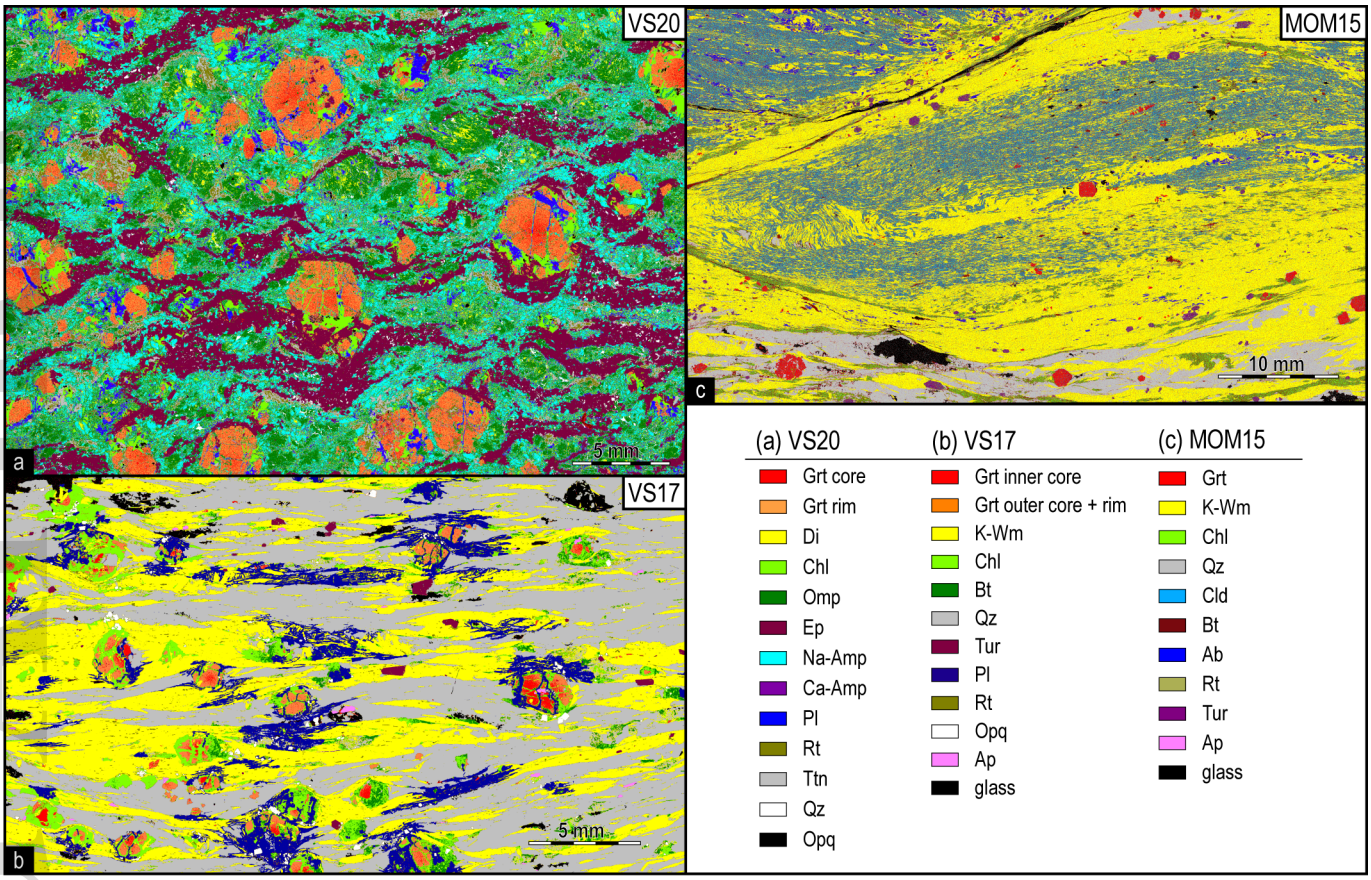

jmg_12574_f4.png

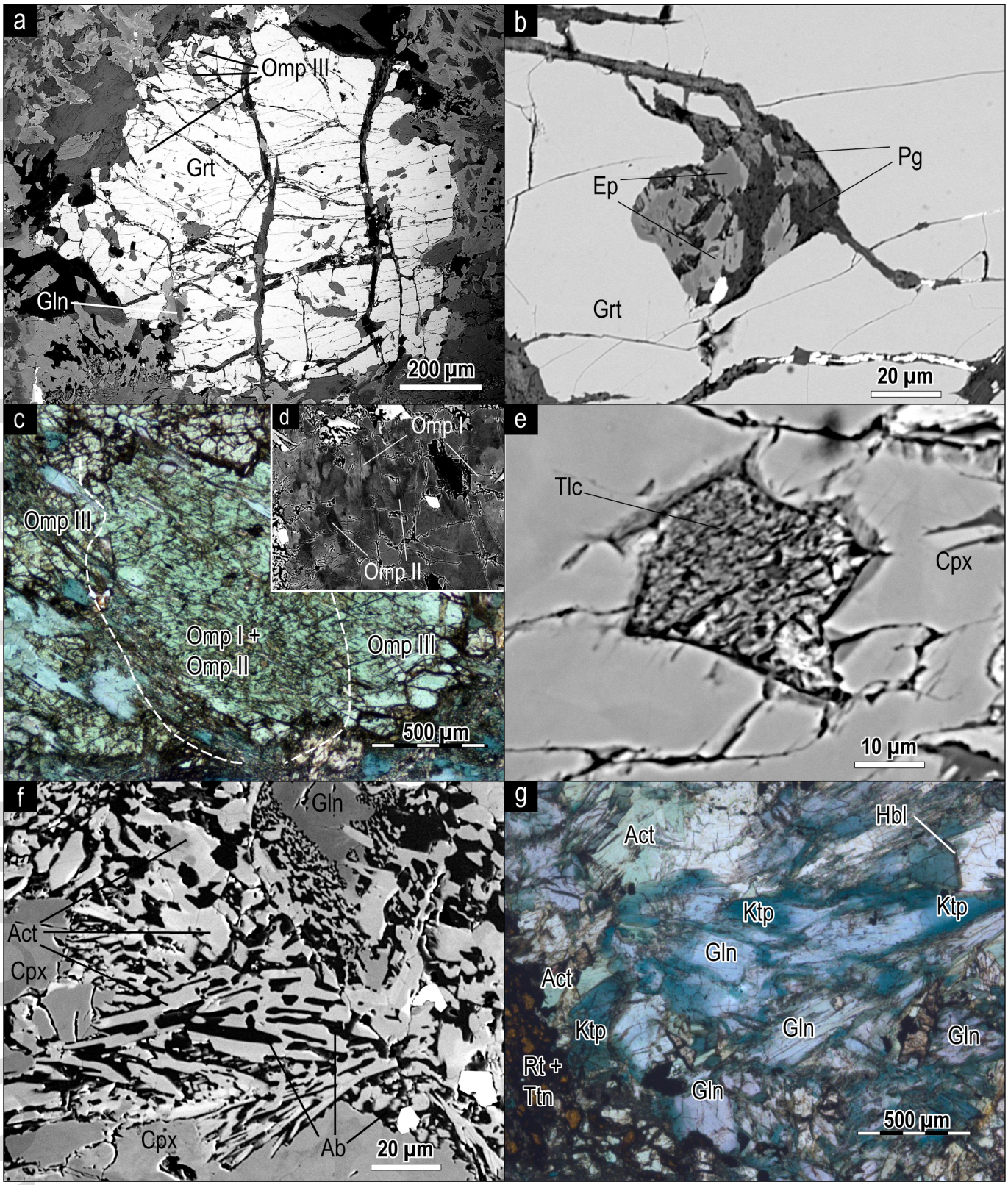

jmg_12574_f5.png

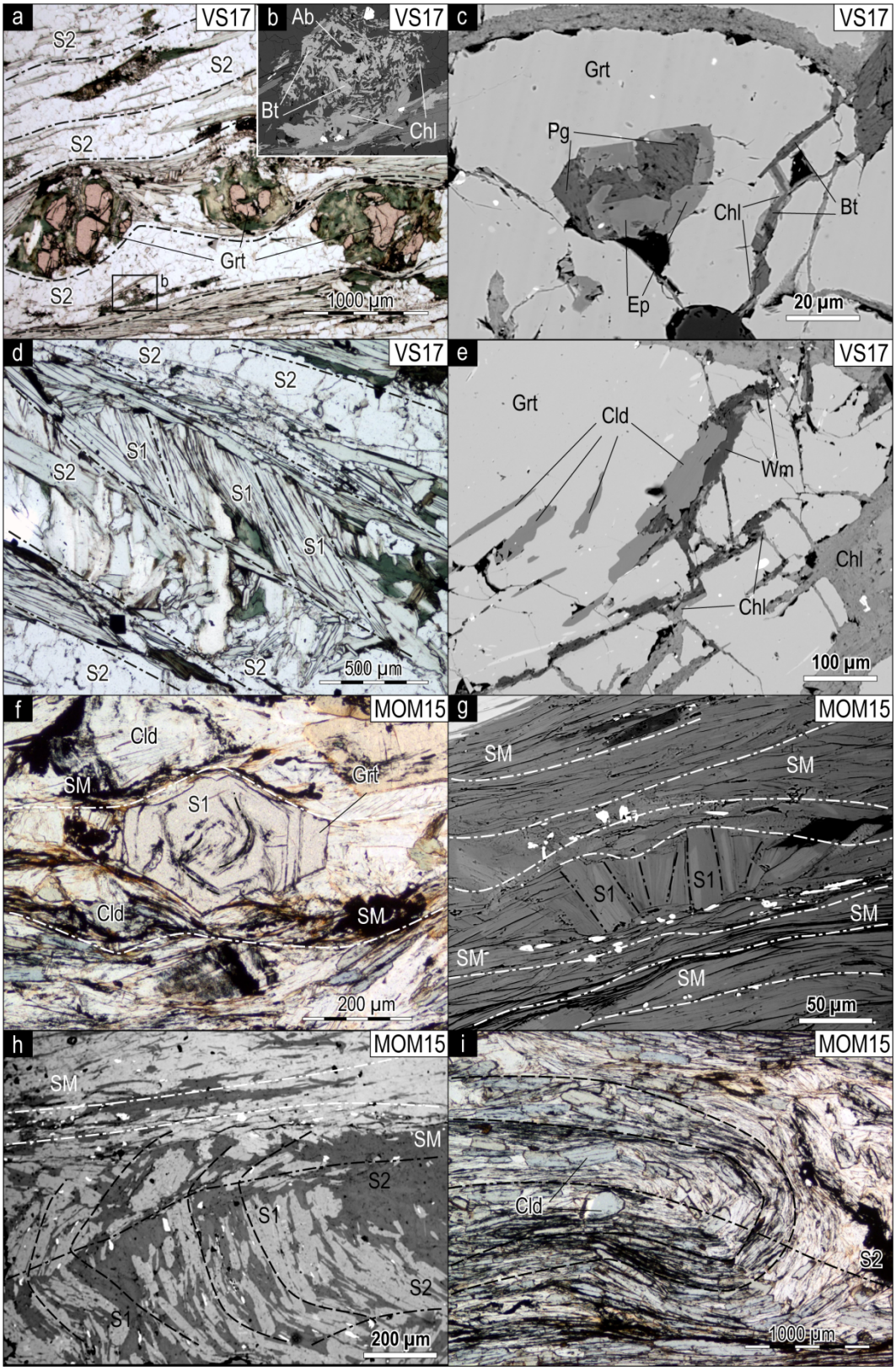

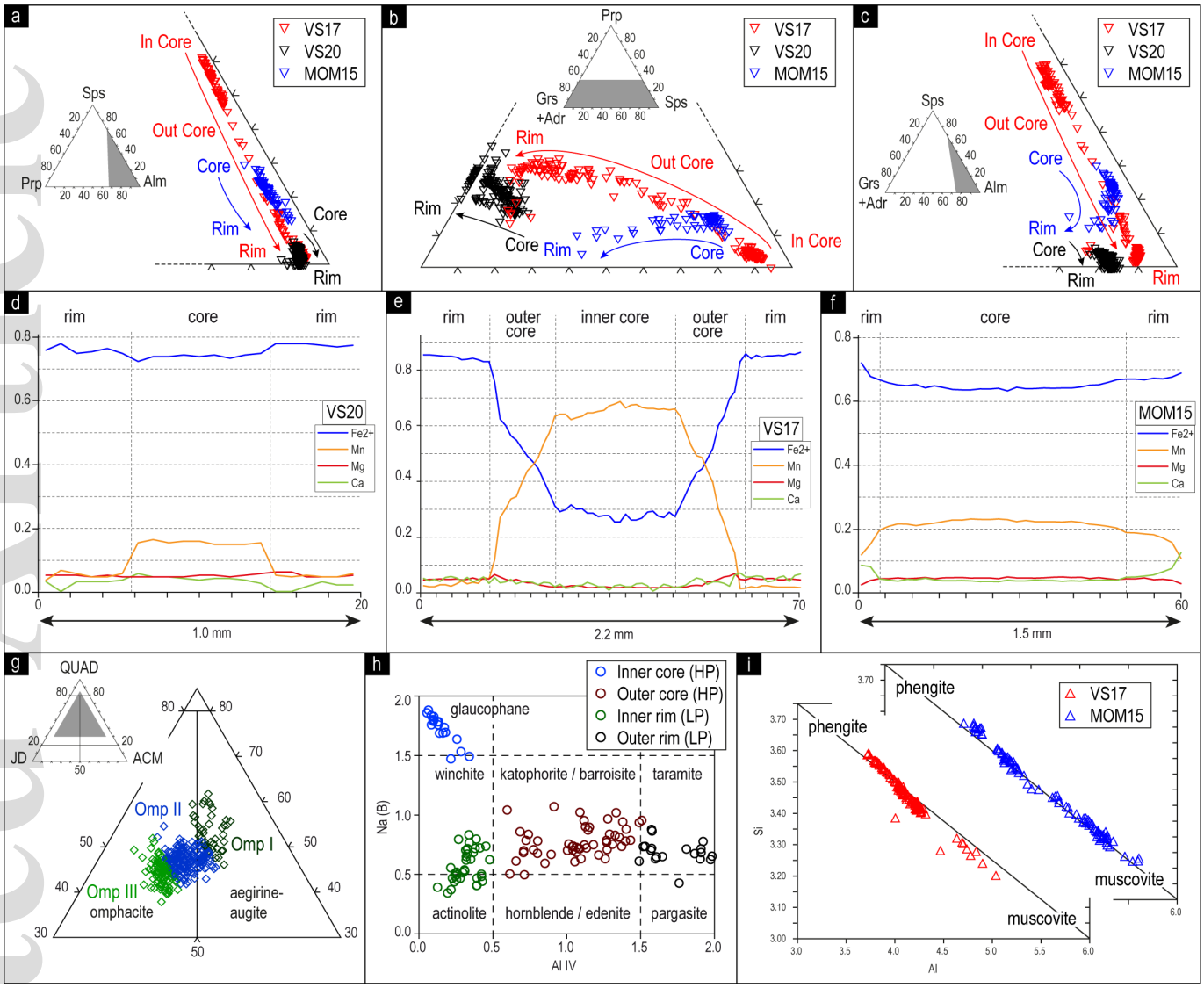

jmg_12574_f7.png

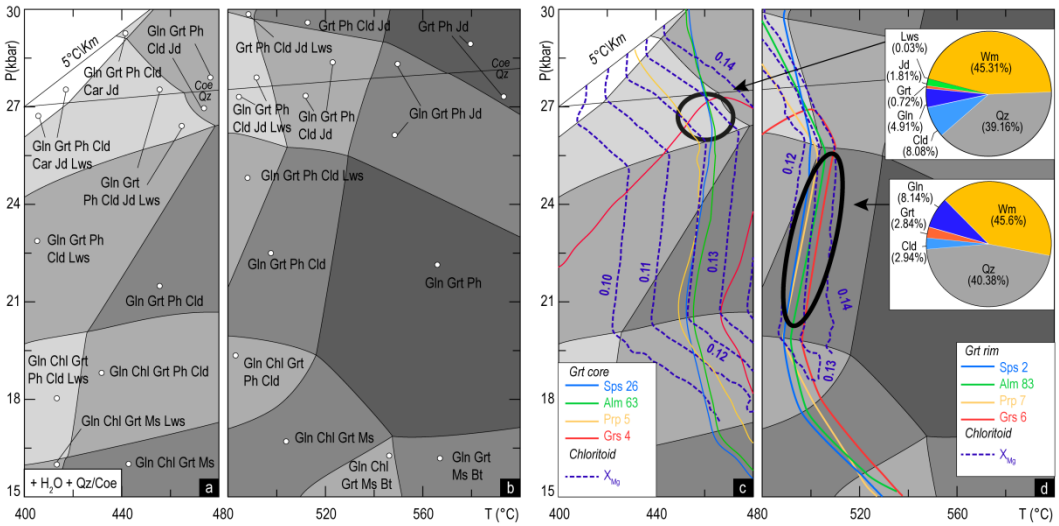

jmg_12574_f8.png

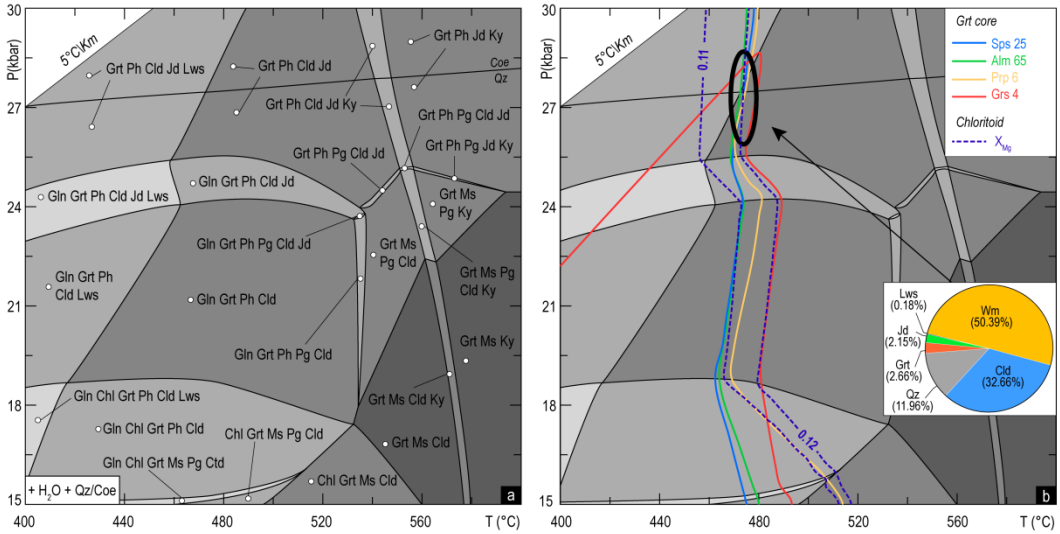

jmg_12574_f9.png

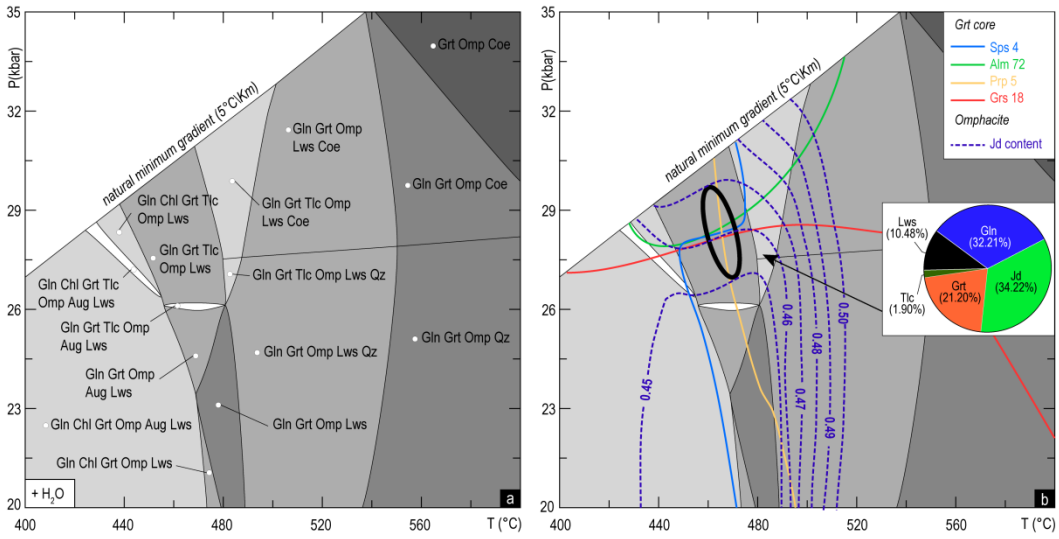

jmg_12574_f10.png

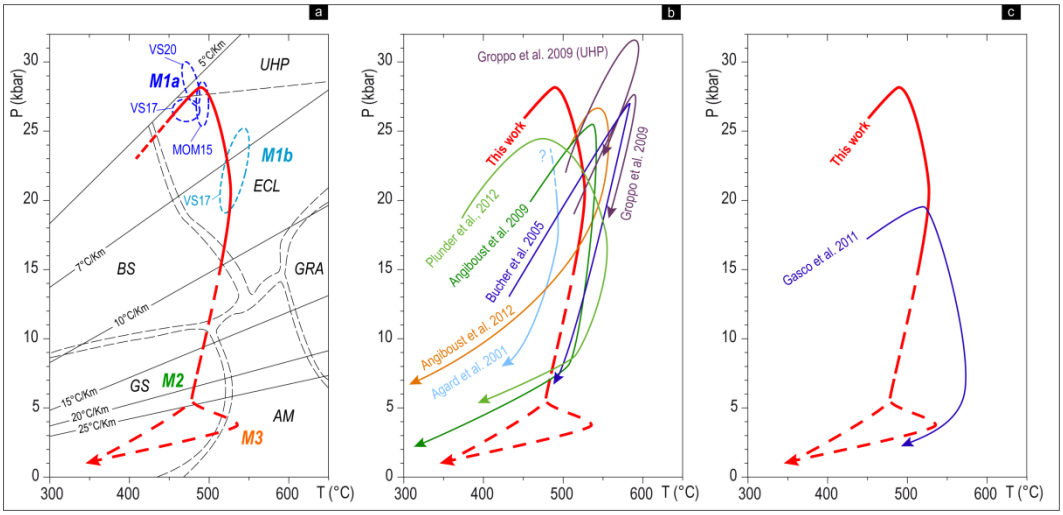

jmg_12574_f11.png